This is a preprint, the final version is subject to change, of the American Mineralogist (MSA)
Cite as Authors (Year) Title. American Mineralogist, in press.
DOI: https://doi.org/10.2138/am-2019-6673

6673 Revision 1

Reconstruction of residual melts from the zeolitized explosive products of alkaline-mafic volcanoes

Linda S. Campbell[1]*, Guido Giordano[2], Michael J. Stock[3], Alessio Langella[4], David L. Bish[5], and G. Diego Gatta[6].

[1]*Geo-Unit 16315, PO Box 4336, Manchester, M61 0BW, U.K.*

[2]*Dipartimento di Scienze Geologiche, Università degli Studi di Roma Tre*, *Largo San Leonardo Murialdo, 1, I-00146, Roma, Italy.*

[3]*Department of Earth Sciences, University of Cambridge, Downing Street, Cambridge, CB2 3EQ, U.K.*

[4]*Dipartimento di Scienze e Tecnologie, Università del Sannio, via de Sanctis, 82100 Benevento, Italy.*

[5]*Department of Earth and Atmospheric Sciences, Indiana University, Bloomington, IN 47405, U.S.A.*

[6]*Dipartimento Scienze della Terra, Università degli Studi di Milano, Via Botticelli 23, I-20133 Milano, Italy.*

*Corresponding author

Keywords: pyroclastic deposits; fractional crystallization; natural zeolites; magmatic model; volcanology; Colli Albani.

Highlights:

This is a preprint, the final version is subject to change, of the American Mineralogist (MSA)
Cite as Authors (Year) Title. American Mineralogist, in press.
DOI: https://doi.org/10.2138/am-2019-6673

- Pyroclastic fine ash reveals a more evolved melt fraction of significant quantity, immediately prior to explosive eruption.
- Magmatic mineral assemblage and compositions closely predicted with model.
- Preservation of melt SiO_2/Al_2O_3 ratio demonstrated in zeolitization of volcanic glass.
- Results validated by independent natural and experimental data.

Abstract

Magmatic conditions prior to explosive eruption are often investigated using geochemical signatures in glassy components of pyroclastic deposits and related to magmatic processes at depth. One important process is fractional crystallization, which causes systematic changes to the SiO_2/Al_2O_3 ratio of the residual melt as can be determined by observation of the mineralogy of fully crystallized lavas, by experimental petrology, and by magmatic modelling. However, for many alkaline-mafic pyroclastic deposits the record of residual melt compositions is obscured by alteration, commonly affecting more than 50% of pyroclastic rock components including reactive glass and some susceptible minerals. In this study, melt signatures of SiO_2/Al_2O_3 represented heterogeneously by scarce fresh glass and abundant, zeolitized proxy-glass in the alkaline deposits of a major, caldera-forming eruption were used in conjunction with a model system (Rhyolite-MELTS) to reconstruct residual melt compositions and characteristics that existed immediately prior to explosive eruption. Through the model, full major oxide compositions of residual melts and fractionally crystallizing minerals become accessible, with associated constraints on volatiles and physical characteristics (melt temperature, density, viscosity). The use of zeolitized proxy-glass signatures relies on established and deposit-specific evidence for 'hydrologically closed' systems that suggests the SiO_2/Al_2O_3 ratio is closely retained through

initial alteration reactions and therefore closely representative of SiO_2/Al_2O_3 in the precursor glass (erupted melt). The relationship is supported by a review of available, paired data (r^2=0.94). Therefore, magmatic system data for the abundant and pervasive fine ash fraction of pyroclastic deposits can be investigated using this method, and can progress more deeply beyond the widely used simple affiliation to igneous rock classification. Model-predicted magmatic mineral compositions (clinopyroxene, spinel and nepheline as demonstrated here) serve to validate a case study reconstruction by comparison with compositions reported from natural and experimental samples. This predictive capability of the novel procedure is demonstrated in the case of a major caldera-forming eruption, the 355 ka Villa Senni event of the quiescent Colli Albani volcano, Rome, Italy, and its pervasively zeolitized *Tufo Lionato* deposit (>50 km^3). The key finding is that a more evolved residual melt fraction has been revealed, based on a reconstructed SiO_2/Al_2O_3 ratio of 2.05 relative to that of the parent magma at 2.68, with implications for reappraisal of pre-eruptive conditions and eruption mechanisms, and potentially for similar patterns across the volcanic stratigraphy and for other alkaline volcanoes.

Introduction

Alkaline-mafic volcanoes present many questions about controls on the style of their eruptions and magmatic storage conditions in the shallow crust (Cashman and Giordano, 2014). Based on the premise that pre-eruptive processes relating to fractional crystallization in particular form an essential part of that understanding, this study addresses the accessibility and utilization of geochemical records of fractional crystallization in alkaline-mafic pyroclastic rocks. 'Accessibility' of geochemical records is highlighted because demonstrating the integrity of SiO_2/Al_2O_3 signatures in altered (zeolitized) former glass components of pyroclastic deposits (as

shown here) is fundamental to consideration of their use as proxies for quenched, fractionally crystallized melts. 'Utilization' applies to SiO_2/Al_2O_3 signatures for both fresh and proxy glass components. A novel procedure is introduced which enables the reconstruction of residual melt characteristics and compositions occurring immediately prior to explosive eruption, through the use of pervasive, fine ash SiO_2/Al_2O_3 signatures combined with magmatic modelling.

Volcanic deposit records

Records of the progression of magmatic crystallization are readily available from the mineralogy and petrology of effusive volcanic products (lavas) but are more elusive in heterogeneous explosive products (pyroclastic deposits) because of incomplete crystallization of melt fractions and fragmentation of all components. This is especially true when residual glass components have been altered, replaced by abundant, pervasive zeolitic and argillic assemblages (e.g., de'Gennaro and Langella, 1996, Hay and Sheppard, 2001, Dai et al., 2017). However, as the SiO_2/Al_2O_3 ratio in zeolite mineral products generally reflects that of their reactants in hydrologically 'closed' systems (Langella et al., 2001 and below), the SiO_2/Al_2O_3 ratio can be used as a proxy-glass signature, subject to effective characterization and understanding of the alteration reactions.

Zeolitic Alteration and Proxy Glass

Controls on alteration assemblages for volcanic deposits, including the influence of SiO_2/Al_2O_3 ratios in precursor reactant phases (minerals, glasses), are reviewed in Bish and Ming (2001). The reaction environment of a pyroclastic deposit comprises multiple solid phases as well as a vapor or aqueous reactant that can be a transitional gel phase, often reported from experimental studies (e.g. de'Gennaro et al., 1999). Glassy reactants may be particles of pumice, scoriae or glass shards, with or without microphenocrysts. Mineral reactants may be crystal

fragments originating from the magma or as component parts of inherited lithic clasts. Thus, where the petrographic context is well understood, paired reactant and zeolite compositions can be used to construct specific reaction equations for mass balance evaluation. These fundamental equations were determined by pioneering work in the 1960's and 1970's, which tested theoretical concepts with experiments and natural assemblages (e.g. Sheppard and Gude, 1968; Hay, 1964; Eugster, 1969; Surdam and Eugster, 1976).

Experimental studies on the zeolitization of natural volcanic glasses are very informative. They have determined that pH, influenced by Mg^{2+}, can affect the fate of Al in the alteration assemblage (Gottardi, 1989; de'Gennaro et al., 1999; Ghiara and Petti, 1995). This effect is due to hydration of Mg^{2+} to form octahedrally coordinated layers (brucite), raising the H^{+}/Mg^{2+} ratio in the solution and thereby lowering its pH. Octahedrally coordinated Al^{3+} (gibbsite) is more stable at low pH, and smectite crystallization is promoted. But as alteration reactions progress, the fluid-pH increases due to alkali cation buffering, and zeolites quickly become stable and dominant (many natural examples are reviewed in Langella et al., 2001). Nevertheless, other controls such as a high fluid/rock ratio or external fluid buffering observed in more open, natural systems may reduce zeolitic-SiO_2/Al_2O_3 relative to the precursor glass-SiO_2/Al_2O_3. For example, Surdam and Parker (1972) showed that SiO_2 can be preferentially mobilized into the fluid phase at high pH with open-system brine involvement. Broxton et al. (1987) and Vaniman et al. (2001) reported alteration reactions involving high-Si external groundwaters, releasing excess SiO_2 as opal or cristobalite as part of the secondary assemblage. Temperature exerts an additional external control on reaction products, and this has been shown to govern the crystallization of authigenic feldspars over zeolites in the hotter parts of the Campanian Ignimbrite, southern Italy (Langella et al., 2013). The exchangeable cation ratios in zeolites can be influenced

113 independently of framework SiO_2/Al_2O_3 inherited from the glassy precursor, as demonstrated in
114 Cappelletti et al. (2015) for limestone clast reactions in an Italian pyroclastic deposit (from the
115 Sabatini volcano). Post-zeolitization external fluid interactions are inevitable in longer geological
116 histories, and low SiO_2/Al_2O_3 zeolites are especially susceptible to further reactions. These can
117 be difficult to identify because of progression to felsic and argillic assemblages (Etame et al,
118 2009; Campbell et al., 2012; Vignaroli et al., 2015). Overall, reaction conditions that govern
119 zeolite assemblages are fundamentally explained by mineral stability constraints (Chipera and
120 Apps, 2001).

121 A review of currently available, worldwide data (Supplementary 1, Figure S1 and Table
122 S1.1) confirms a general relationship of zeolite products to reactants (SiO_2/Al_2O_3) in volcanic
123 deposits. At present, paired examples of zeolite products and reactants are scarce due to the
124 difficulty of retrospective pairing and to analytical challenges (Campbell et al., 2016). However,
125 a strong correlation of ratios between reactants and products is found ($r^2 = 0.94$), particularly for
126 known glassy reactants in hydrologically 'closed' systems (i.e. where zeolitization reactions take
127 place with minimal loss or gain of H_2O in the deposit, Langella et al., 2001). Young
128 phreatomagmatic environments are good examples of such closed systems, and the term
129 'geoautoclave' as explained by Langella et al. (2001) is particularly relevant to the data from the
130 Italian pyroclastic reaction environments (Supplementary 1, Figure S1, Table S1.1), including
131 the case of Colli Albani presented in this study. A general margin of error relating to complex
132 controls on reactant to zeolite SiO_2/Al_2O_3 as outlined above, is estimated as <5% from the closed
133 system data in Figure S1. The lowest SiO_2/Al_2O_3 signatures in Figure S1 are represented by very
134 silica-undersaturated reactant phases such as foiditic and nephelinitic glasses (sources in Table
135 S1.1). Such extreme quenched-melt compositions are expected to be unstable in vapor-present,

pyroclastic depositional environments, reacting quickly to form secondary assemblages of minor smectite, low-Si zeolites (phillipsite and chabazite series') and Fe oxides/hydroxides. This pattern of secondary mineral paragenesis is extensively documented for many alkaline volcanic reactants (Gottardi, 1989; Ghiara and Petti, 1995; de'Gennaro et al., 1999; Chipera and Apps, 2001; Hay and Sheppard, 2001; Etame et al., 2012). It is also consistent with reports of quench problems in experimental magmatic studies of volatiles in highly alkaline melts, some with specific mention of zeolite crystallization (Behrens et al., 2009; Shishkina et al., 2014; Vetere et al., 2014; Fanara et al., 2015).

In summary, reactant SiO_2/Al_2O_3 ratios are well preserved in zeolite mineral products and are largely unaffected by subsequent non-framework cation exchange. This presents a powerful opportunity to apply the signatures as proxy-glass ratios to access full compositions of explosively erupted fractional melts, not previously recognized.

Volcanological Implications (Application)

Past alkaline-mafic pyroclastic events and present-day volcanic hazards are well known in the Mediterranean region, yet SiO_2/Al_2O_3 ratios from ash components in hundreds of km^3 of altered deposits (typically 30-80% zeolitized in Italy, de'Gennaro and Langella, 1996) have not previously been used to link *directly* and *specifically* to pre-eruptive magmatic fractionation. The basis and significance of our approach is that crystal fractionation and its impact on other shallow-chamber processes contributes profoundly to pre-eruptive outcomes, not least in its effect on compositions of residual melts. Thus, when a glass or zeolitic proxy-glass SiO_2/Al_2O_3 signature is compared with a modelled SiO_2/Al_2O_3 profile of the fractionating melt it is possible to access multiple characteristics of that melt and its crystallizing minerals (i.e. modelled output datasets). This presents an ideal opportunity for validation of the output data, as modelled

mineral compositions can be compared directly with analyzed sample compositions. Neither the determination of former-glass SiO_2/Al_2O_3 from the secondary zeolite minerals nor the determination of melt characteristics from magmatic modelling are novel, but their combined use in pinpointing and reconstructing melt evolution at the moment of quench (explosive eruption), using the single, yet robust and sensitive parameter of the SiO_2/Al_2O_3 ratio, has not previously been attempted or considered.

The fundamental pre-requisites for this approach are: (a) a detailed volcanological reference framework (geometry, stratigraphy, compositions); (b) evidence of system phase relationships (magmatic mineralogy and textures); and (c) compositional data for all types of glassy or former-glass (zeolitized) components found in the heterogeneous pyroclastic deposits, representing various erupted melt components from an assumed common source. It follows that the best opportunities to utilize this application will be for volcanoes with a good record of both effusive and pyroclastic eruptions, as fully crystallized lavas provide essential reference data on changing mineral-melt phase relationships and mineral compositions along a natural cooling path. It also follows that the most significant and substantive value from this melt-reconstruction opportunity will be in cases where glass compositions are most susceptible to zeolitic alteration, such as volatile-enriched, alkaline, silica-undersaturated rocks. No restrictive assumptions are required concerning the potential nature of the magma storage region, which could be complex (Cashman and Giordano, 2014, Annen et al., 2015, Cashman et al., 2017), and which could contribute to heterogeneity of pyroclastic components (e.g. potential pre-eruptive magma mingling or mixing due to recharge from a common source). Indeed, our worked example from deposits of the caldera-forming Villa Senni eruption (355 ka) of the currently quiescent Colli

Albani volcano (Rome, Italy) is representative of an extremely complex system sustaining many unresolved scientific questions (Funiciello and Giordano, 2010).

Worked example – The Villa Senni eruption, Colli Albani, Italy

Geological context

The Colli Albani volcano, Rome, forms part of the Roman Magmatic Province and is described in depth in a thematic volume by Funiciello and Giordano (2010). It presents ongoing hazards for the highly populated capital city of Rome (Carapezza et al., 2010, Giordano et al., 2010, Ciotoli et al., 2013). The Roman Magmatic Province is part of the active convergent zone between the African and Eurasian plates, a back-arc, thin-crust mantle wedge setting with a high flux of heat and CO_2 (Mattei et al., 2010; Giordano et al., 2014; Avanzinelli et al., 2017). Carbonate melts are known, and although their origins are controversial (Stoppa and Woolley, 1997; Downes et al., 2002; Cross et al., 2014; Gozzi et al., 2014), isotopic evidence supports sediment recycling (Cavarretta and Lombardi, 1990; Conticelli and Peccerillo, 1992; Avanzinelli et al., 2009; Conticelli et al., 2015). The province is characterized by K-rich alkaline magmas and has an overall age profile of Miocene in the north-west (Tuscany-Corsica) to present-day activity in the south-east (the Neapolitan volcanoes of Campania).

The earliest activity of the Colli Albani volcano is dated at 608 ka (Karner et al., 2001; Gaeta et al., 2016), and the magma chamber is situated at about 6 km depth (Boari et al. 2009). All erupted rocks from this volcano are compositionally similar; highly potassic and silica undersaturated (typically foidites and tephrites, ~8-12 wt% alkalis and <<52 wt% SiO_2, Trigila et al., 1995; Boari et al., 2009; Conticelli et al., 2010), with important roles for mixed volatiles (Freda et al., 2008). Magmatic and metasomatic enclaves and xenoliths in the deposits are

attributed to complex interactions of the magma with the shallow crust and provide insights on H_2O-CO_2-dominant volatile sources (de Benedetti et al., 2010). Despite considerable heterogeneity in erupted components of the pyroclastic deposits, the overall geochemical similarity of whole rock analyses throughout the succession implies derivation from a common magma source (Palladino et al., 2001). This similarity presents valuable opportunities to compare fully crystallized lavas with different components of the pervasively zeolitized pyroclastic rocks. Specifically, two relevant aspects of the magmatic mineralogy are (i) that phenocrystic leucite and clinopyroxene were dominant in the early crystallization stages of these magmas (Palladino et al., 2001), consistent with a cotectic path defined in experimental studies (Freda et al., 1997, 2008); and (ii) that plagioclase crystallization was suppressed due to high CO_2 partial pressure sustained by degassing of a metasomatized mantle source (Conticelli et al., 2015). Together, these magmatic controls present a cooling system that preferentially concentrates incompatible elements (conspicuously, Sr), volatiles and Al into the melt phase relative to those in the source magma.

Field and stratigraphic context

Three main stages in the evolution of the Colli Albani volcano are recognized (Giordano et al., 2010); (i) Vulcano Laziale (600-355 ka); (ii) Tuscolano-Artemisio-Faete (355-180 ka); and (iii) Via dei Laghi (200 ka to present). Both effusive and pyroclastic eruptions have occurred throughout the history of the volcano, but phreatomagmatic activity has dominated the third stage. The Villa Senni eruption was a major caldera-forming, explosive event that marked the end of the first stage. This is the focus of the present case study.

The Villa Senni eruption deposited the *Tufo Lionato* (VSN_1) and *Pozzolanelle* (VSN_2) ignimbrites over an area of 1600 km^2, with a deposit volume estimated in excess of 50 km^3

(Giordano et al., 2010, and Figure 1). This stratigraphic relationship is significant for providing an understanding of the alteration environment, as the upper *Pozzolanelle* unit is unzeolitized. It provides evidence that the underlying *Tufo Lionato* unit was quickly insulated from meteoric and surface fluid sources, thereby supporting an internal (magmatic) origin for the alteration volatiles in a geoautoclave-type environment (Langella et al., 2001). Further evidence for this lies in the uniformity of the deposit in terms of its pattern of alteration (de'Gennaro et al., 1995; de'Gennaro and Langella, 1996; Watkins et al., 2002; Giampaolo et al., 2008; and Giordano et al., 2010).

The pyroclastic deposits of Colli Albani are typically pervasively zeolitized, consistent with the regional pattern for Roman Magmatic Province pyroclastics (de'Gennaro and Langella, 1996). However, their whole-rock compositions are similar to the lavas of Colli Albani as described above, with leucite, clinopyroxene, mica, and rarely apatite as crystal fragments in the pyroclastics, among scoria clasts and the zeolitized matrix. In places, external fluid interactions are evident from localized, distinctive changes in geochemistry and mineralogy towards argillic assemblages, but these features have been shown to post-date the zeolitization (Vignaroli et al., 2015).

Investigation methods

Reference samples (The 'known system'). The *Vallerano* 'LLL' lava (460 ka, Karner et al., 2001, Giordano et al., 2010, Gaeta et al., 2016), represented by sample data VLS05 (Boari et al., 2009 and Figure 1), was selected to serve as the benchmark magmatic reference for the known geochemistry and mineralogy of the pre-caldera system. An initial empirical evaluation of the overall change in SiO_2/Al_2O_3 during crystallization was made using the reported mineralogy: clinopyroxene and leucite (phenocrysts and groundmass), and groundmass olivine,

magnetite, mica, haüyne, apatite and nepheline ± melilite (Conticelli et al. 2010). A further advantage of this lava is that it has yielded crystals of zeolites; "*milky white* [chabazite] *crystals twinned with spherical shape, diameter 1-5 mm in leucitite with phillipsite"* (Passaglia, 1970). The chabazite compositions (Passaglia, 1970) serve as direct witnesses to fluid reactions with lava components, and hence to a closer understanding of the compositions of contributing reactant phases.

Pyroclastic deposit samples (The 'questioned system'). Samples of the *Tufo Lionato* ignimbrite (VSN_1) selected for the present study include one from the Imater quarry ('Imater-AGLOO' described in Vignaroli et al., 2015), one from an exposure at Fioranello ('IT16' ~1km from Imater), and a third from Villa Adriana ('IT118'), near Tivoli, on the eastern side of the volcano (Figure 1). Petrographic observation was undertaken by optical microscopy and X-ray mapping to evaluate the paragenesis and to select suitable areas for quantitative analysis, mainly of the pervasive, zeolitized matrix (former glassy fine ash) component of the rock but also of pumice or scoria-associated zeolites. Mineral compositions (chabazite and phillipsite series') were then determined by electron probe microanalysis (EPMA) using a defocused beam (10 and 20 μm) and the 2nA, 15kV, alkali-prioritization and data reduction recommendations of Campbell et al. (2016). Wavelength dispersive spectrometry (WDS) was justified over energy dispersive spectrometry (EDS) for both spot analyses and X-ray mapping of zeolites in this context of heterogeneous pyroclastic components, based on analytical challenges of Sr-Si and Ba-Ti interferences and considerable beam interaction effects on the alkalis and volatiles, as evaluated in Campbell et al. (2016). Mineral proportions using representative bulk samples of the *Tufo Lionato* deposit were determined by powder X-ray diffraction (XRD) with Rietveld full-profile fitting (Bish and Post, 1993).

Magmatic modelling (The 'theoretical system'). Thermodynamic modelling of the magmatic system was undertaken using 'Rhyolite-MELTS' software (Gualda et al., 2012). The major oxide composition of the *Vallerano* lava (i.e. the selected, pre-caldera system benchmark composition), was used as a model starting composition (sample VLS-05 of Boari et al., 2009). Models were run at 300 MPa based on the reported depth of the pre-caldera magma chamber (~6 km, Boari et al., 2009). The water content of the magma and the oxygen fugacity were taken as H_2O=2 wt% and fO_2=NNO, after Freda et al. (2008). Cooling path attributes during fractional crystallization were then calculated with the model, producing output datasets of residual melt compositions (major oxides and H_2O wt %), physical characteristics of the melt (viscosity, density, temperature, pressure), crystallizing mineral compositions and crystallization sequence. Important limitations for highly potassic and CO_2-bearing systems are considered in the discussion.

Results

Petrography and texture-compositional features. Pyroclastic components of *Tufo Lionato* are illustrated in Figure 2(a), including some angular crystal fragments with sharp grain boundaries. Some of the juvenile clasts (scoria, pumice, shards) are recognized in terms of those described in Vinkler et al. (2012), notably with respect to their descriptions of 'sc1' (scoria with rounded vesicles) and 'sc2' (scoria with irregular vesicles and microlites). Compositional differences relating to glassy clast texture were determined using X-ray maps (Figures 2b, 3 and Supplementary 1, Figure S2). The Fe distribution in Figure 2(b) best illustrates one aspect of this, which is indicative of higher Fe content in the scoria clast on the left relative to one on the right, as well as showing the general absence of Fe in the zeolitized matrix. The matrix is noted as Al-rich in the Al X-ray maps and is where most Sr in the rock resides (Figures 3 and Supplementary

296 1, Figure S2). In Figure 2(c and d), zeolite crystal morphologies can be seen relating to probable
297 phillipsite series (Figure 2c) and probable chabazite series species (Figure 2d), both within a
298 vesicle-rich yellow pumice clast. However, such examples, especially of rhombic forms of
299 chabazite, are rare due to space constraints in most vesicles. Previous studies on Italian zeolites
300 (for example, de'Gennaro and Langella, 1996), have determined that zeolites occurring in
301 pumice/scoria vesicles tend to be dominated by phillipsite, and those constituting the pervasive,
302 fine, interstitial matrix, are mainly chabazite.

303 **Mineralogy.** X-ray diffraction data from which specific mineral proportions were
304 determined for a representative sample of *Tufo Lionato* (Fioranello locality) are provided in
305 Table 1 and Supplementary 1, Figure S3. Magmatic minerals detected in the sample were leucite
306 (9 wt%), diopside (8.1 wt%), phlogopitic mica (6.4 wt%) and nepheline (0.8 wt%), consistent
307 with a *Vallerano*-like system in which phenocrysts of leucite and diopside are produced with
308 phlogopite, but no feldspars. The substantial alteration assemblage comprised chabazite 42 wt%,
309 phillipsite 22 wt% and smectite-group minerals (not quantified). Analcime at 2.3 wt% was
310 considered as secondary after leucite. Based on independent textural and deposit-scale studies
311 (de'Gennaro et al., 1995; de'Gennaro and Langella, 1996; Watkins et al., 2002; Giampaolo et al.,
312 2008; and Giordano et al., 2010), it is widely considered that the matrix zeolite of *Tufo Lionato*
313 represents an alteration product of the abundant and pervasive 'former glassy ash' resulting from
314 the caldera-forming Villa Senni eruption. The distribution of the zeolitized matrix in the
315 Fioranello and Villa Adriana samples is particularly well shown by their respective Al X-ray
316 maps (Figures 3 and Supplementary 1, Figure S2), supporting this view.

317 Representative zeolite compositions and comparative data are listed in Table 2, with a
318 full set of analyses given in Supplementary-2, Table S2.1. Independent comparator compositions

of *Tufo Lionato* zeolites based on separated bulk samples (de'Gennaro et al., 1995), and from two other studies (Passaglia and Vezzalini, 1985; Passaglia et al., 1990), match closely with our microprobe dataset. As the present study focusses on the pervasive matrix, it is presumed that most data represent chabazite series compositions (see de'Gennaro and Langella, 1996). Nevertheless, a few analyses were collected from pumice zeolites displaying crystal-cluster textures typical of the phillipsite series (e.g. Figure 2c). In a ternary representation of the $R^{+}R^{++}Si$ components of the *Tufo Lionato* zeolites (Figure 4a), no clear differences between chabazite and phillipsite series' compositions, nor between the separate sample localities, or pumice versus matrix, were observed. Yet subtle variations in non-framework cations are detectable in the cation ratio representations of Figs. 4b and 4c. The zeolites are classified as chabazite-K, chabazite-Ca, phillipsite-K and phillipsite-Ca, based on their dominant, non-framework cation compositions (after Coombs et al., 1997). Individual analyses are labelled accordingly in Tables 2 and S2.1. The contribution of Sr^{2+}, though insufficient to warrant classification as chabazite-Sr, is significant in the zeolites of the Colli Albani deposits and therefore merits further graphical expression (Fig. 4c). In both Figs. 4b and 4c, minor involvement of an external Ca-Na fluid from the base of the deposit, with no detectable influence on zeolitic SiO_2/Al_2O_3, is hinted at in the IT118 Villa Adriana sample data. Using spatially precise spot analyses and X-ray maps from this microprobe dataset (Table S2.1 and Figure 3), compositional zonation expressed by M^{2+} cation variations in matrix zeolite (assumed mainly chabazite) is apparent.

Overall, the compositions of pervasive *Tufo Lionato* zeolites are striking for two reasons; first, their very low Si:Al ratios (expressed as oxide ratios in this application for ease of comparison with potential reactant phases), and second, their high concentrations of SrO ≤6

342 wt%. Both characteristics are unusual in the context of currently known, worldwide
343 compositions (Deer et al., 2004), but are most similar to the chabazites of Passaglia (1970) that
344 were hosted by the pre-caldera lavas (*Vallerano, Acquacetosa*, *Casal Brunori* and *Osa* localities,
345 see Table S2.1 and Fig.4). Collectively, petrographic and compositional data from the present
346 study are aligned with several additional analyses and descriptions of the *Tufo Lionato* deposit
347 (Passaglia and Vezzalini, 1985; de'Gennaro and Franco, 1988; Passaglia et al., 1990; de'Gennaro
348 et al., 1995; de'Gennaro and Langella,1996; Watkins et al., 2002; Giampaolo et al., 2008; and
349 Giordano et al., 2010), providing strong evidence for deposit-scale homogeneity and
350 reproducibility and strengthening the case for internal, rather than external, constraints on
351 zeolitization (Giordano et al., 2010).

352 **Modelled data.** Cooling path data tables for our benchmark reference melt *Vallerano*
353 (starting composition), the residual melt, and for evolving compositions of clinopyroxene,
354 nepheline, spinel-group minerals and minor silicates, are given in Supplementary-2, Tables S2.2-
355 S2.7. The *Rhyolite-MELTS* model (Gualda et al., 2012) gives a liquidus temperature of 1210°C
356 at 300 MPa for the benchmark *Vallerano* lava, with the crystallizing mineralogy dominated by
357 leucite and diopsidic clinopyroxene. Spinel is theoretically present throughout the modelled
358 sequence, mainly as a solid solution of spinel ($MgAl_2O_4$) and magnetite (Fe_3O_4) components,
359 with minimal ulvöspinel ($Fe(Fe,Ti)_2O_4$). Apatite appears below ~1100°C, and the remaining
360 minerals (very minor garnet, plagioclase and nepheline) all theoretically begin to crystallize
361 below 900°C. The modelled composition of nepheline has a significant kalsilite component
362 (close to 7 wt% K_2O).

363 Table S2.2 provides major oxide compositions and physical attributes of the residual melt
364 with a decreasing temperature during fractional crystallization. In Table S2.2. note especially the

predicted change in SiO_2/Al_2O_3 as crystallization progresses. This represents the SiO_2/Al_2O_3 signature that would be expected in a quenched glass if an explosive eruption occurred at any particular point of fractional crystallization. Therefore, for each incremental change of SiO_2/Al_2O_3 with temperature, multiple characteristics of the modelled residual melt are available.

Application: Residual melt reconstruction

When a fractional crystallization model is well matched to an observed system, modelled data depicting multiple changing parameters of a residual melt can then be accepted as reasonable representations of the real system. For our case study application, Table 3 provides published whole-rock compositions of the pre-caldera *Vallerano* lava and the *Tufo Lionato* pyroclastic deposit (Boari et al., 2009) and gives the average composition of chabazite proxy-glass in *Tufo Lionato* (this study). Figure 5a (right y-axis) presents the SiO_2/Al_2O_3 signature (2.05) of chabazite in combination with the model-determined cooling profile of SiO_2/Al_2O_3 in the residual melt. The quench signature is interpreted to represent the stage of fractional crystallization reached when the explosive, caldera-forming Villa Senni eruption occurred. Note that this represents a more evolved melt phase than those determined from the signatures of scarce fiammae of previous studies (Freda et al., 1997, Gaeta, 1998, Marra et al., 2009, and in the *Validation* section, below).

Once the melt composition at the time of eruption is determined, model-output data are accessed: (i) the full major oxide composition of the residual melt (Supplementary-2, Table S2.2); (ii) compositions of minerals crystallizing from this melt (Supplementary-2, Tables S2.3-2.7); and (iii) physical characteristics of the melt (Supplementary-2, Table S2.2, and Figure 5b). Figure 5b illustrates that melt viscosities are sensitive to the initial volatile budget (see Giordano et al., 2008), and change more significantly with crystallization of the late-fractionates (felsic

minerals and apatite) than with crystallization of phenocrystic leucite and clinopyroxene. It is also notable that H_2O concentrations in the melt increase dramatically below ~900°C, but as the current model does not allow for vapor saturation (due to limited volatile solubility data for alkali systems in Rhyolite-MELTS; see discussion in Stock et al., 2016), and does not directly account for other mixed volatiles (C, F, Cl, S) or their chemical speciation, interpretation at this stage is not appropriate. Nevertheless, research development opportunities for elucidating mixed volatile behaviors based on our modelled compositional outputs are outlined below.

Discussion

Validation

To test the validity of this new approach, model-predicted melt and mineral compositions are compared with natural and experimental melt and mineral assemblages and their directly analyzed compositions. Figure 6 demonstrates this for the melts, showing the compositional trajectory of the modelled residual melt relative to the whole-rock composition of the pre-caldera *Vallerano* lava (used as the model starting composition). Published whole-rock and fiammae compositions (Boari et al., 2009, Freda et al., 1997, Gaeta, 1998 and Marra et al., 2009) from *Tufo Lionato* are shown for comparison, along with the reconstructed proxy-glass composition of this study (representing the Villa Senni fine ash), and 'reconstructed' natural fiamme compositions (as a test of model output data validity). As volatile saturation is suppressed in the Rhyolite-MELTS model, the compositional evolution of the residual melt does not account for effects of an aqueous phase, causing uncertainty in the lower temperature range (Figure 6), where a fluid phase might naturally exsolve. One of these effects, in particular, would be in the fluid/melt partitioning behaviors of the alkalis. This comparison of melt signatures with

411 independently analyzed data therefore provides a strong case for validity of our modelled output
412 data.

413 The magmatic mineralogy of the modelled fractional crystallization sequence presented
414 in Figure 5a is broadly consistent with the findings of Trigila et al. (1995), Palladino et al.
415 (2001), Freda et al. (2008), Boari et al. (2009) and Conticelli et al. (2010). Phlogopite was not
416 predicted by the model when starting with H_2O at 2 wt%, but it has been produced
417 experimentally at higher pressures and when specific mixed volatiles were added to the natural
418 starting materials from this volcano (500 and 1000 MPa with 2 wt% H_2O, and 500 MPa with 1%
419 H_2O and 3% CO_2, Freda et al., 2008). Although our preliminary model system lacks the volatile-
420 sensitive phases mica and haüyne (Gualda et al., 2012 and Gleeson et al., 2017 discuss model
421 limitations for volatiles), and instead produces garnet and extremely minor plagioclase
422 crystallization at a very late stage, it successfully predicts nepheline, apatite and spinel-group
423 minerals in addition to persistent leucite and clinopyroxene.

424 In Table 4, model-predicted clinopyroxene compositions for a *Vallerano* 'start melt' and
425 the *Villa Senni* 'evolved, erupted melt' determined in this study are listed alongside published
426 natural and experimental clinopyroxene compositions thought to represent similar stages of melt
427 evolution. Most striking in modelled clinopyroxene is the trend of increasing Al and decreasing
428 Mg as the melt evolves during fractional crystallization, with Ca effectively constant except for a
429 small decrease at lower temperature as Na increases (Figure 7). Overall, the pattern of modelled
430 crystal chemical data mirrors that of widely reported clinopyroxene compositions for the Colli
431 Albani deposits, from phenocryst cores that are dominantly diopsidic, towards rims and
432 groundmass occurrences displaying an increasingly aluminous component (Trigila et al., 1995;
433 Conticelli et al., 2010; Gozzi et al., 2014). This suggests not only that the modelled residual melt

compositions of this study are valid, but that the predictive capabilities of resultant, modelled clinopyroxenes can also be tested and used. Full discussions on clinopyroxene crystal chemistry and the Ca-Tschermakitic and aegirine-jadeitic substitution components relevant to these Italian deposits may be found in Morimoto (1989), Hill et al. (2000), Mollo et al. (2013) and Mollo et al. (2016).

Natural nepheline compositions containing a kalsilite component equating to ~9 wt% K_2O (Boari et al., 2009; Conticelli et al., 2010) are also closely predicted by modelled compositions at 7.4 wt% K_2O (this study). Modelled nepheline has 2.2 wt% CaO, similar to reported concentrations in nepheline from some of the younger rocks of Colli Albani (Table 4), but significantly higher than pre-caldera nephelines (0.64 wt% CaO, Boari et al., 2009). One explanation for this discrepancy is that the model did not predict melilite, which is sometimes found in the pre-caldera lavas (Conticelli et al., 2010).

Zeolite analyses from *Tufo Lionato* of this study have been confirmed as being very similar to those of Passaglia and Vezzalini (1985), Passaglia et al. (1990) and de'Gennaro et al. (1995), (Table S2.1). They are also especially close in composition to the Sr-rich, low-SiO_2/Al_2O_3 chabazites hosted in the pre-caldera lavas (*Vallerano,* etc., Passaglia, 1970, Figure 4, and Supplementary 2, Table S2.1). Evidence that the Passaglia (1970) chabazites and younger *Capo di Bove* phillipsites (Galli and Loschi Ghittoni, 1972) grew preferentially from reactants in lava groundmass assemblages is compelling and relevant to this study, and specific reactions are explored below.

Specific alteration reactions – Colli Albani

Chipera and Apps (2001) provided a thermodynamic analysis of geochemical stabilities of zeolite group minerals, but they also emphasized that natural glass-to-zeolite reaction

457 mechanisms are complex, involve metastable transitional phases, and are not completely
458 understood. For the present study of the *Tufo Lionato* deposit, there are multiple compositional
459 references from which to investigate potential reactants, as demonstrated for selected
460 stratigraphic horizons (Supplementary 1, Figure S4). In the figure, evidence that these zeolites
461 are generally recording much more aluminous reactant compositions than indicated from whole-
462 rock and preserved, fresh vitric material, is strong. It is consistent with the working hypothesis
463 that a fractionated, residual melt of 'bulk magmatic groundmass' composition produced, on
464 explosive eruption, a fine-grained matrix of glassy reactants that devitrified rapidly. It is also
465 supported by the requirement for a reactant source of Sr, and neither leucite nor clinopyroxene
466 nor phlogopite fulfil this (partition coefficients in Francalanci et al., 1987; Wood and Trigila,
467 2001; Blundy and Wood, 2003). But potential reasons other than the crystal fractionation
468 hypothesis (Figure 5) are explored in greater depth here.
469 There is some evidence to suggest that alteration of crystal clasts of high-Al phlogopite could
470 have affected the SiO_2/Al_2O_3 ratio of the chabazite if octahedrally coordinated Al was easily
471 mobilized at high pH. Certainly, phlogopite displays alteration textures and it is apparently the
472 only non-vitric precursor source of mobile Ba^{2+} for chabazite ($\leq$8.3 wt % BaO in phlogopite,
473 Boari et al., 2009, and $\leq$0.82 wt % BaO in chabazite, this study). However, the modal
474 proportions of phlogopite, smectite and zeolites in XRD data (Table 1) suggest that phlogopite
475 would be an inadequate source for framework Al needed by the chabazite. A second reason to
476 reject phlogopitic Al is found in the zoned pattern of non-framework cations observed in matrix
477 chabazite. According to normal selectivity sequences of M^{2+} cations entering the chabazite
478 structure, Ba^{2+} is expected first, followed by Sr^{2+} and then Ca^{2+} (Ames, 1961; de Gennaro et al.,
479 2003; Dyer, 2007). However, the highest concentrations of Sr in chabazite are associated with

480 the first-nucleated parts of these zoned minerals (Figure 3 and Supplementary 1, Figure S2),
481 suggesting that different reaction kinetics for different precursors were in control. In other words,
482 the Sr-rich precursor phase reacted faster than the phlogopite. The zonation provides further
483 evidence for the 'immediate' replacement of a former Sr-enriched glass prior to phlogopite
484 reaction.

485 Potential partial reaction equations that satisfy the Passaglia (1970) *Vallerano* chabazite
486 compositions in terms of Si and Al alone, are examined below. They use magmatic mineral
487 'precursor' reactants, singly or in combination, that occur in the *Vallerano* reference lava (Boari
488 et al., 2009; Conticelli et al., 2010).

489 1) $5[AlSi_2] = [Al_5Si_7] + 3Si$
490 Leucite Chabazite

491 2) $5[Al_3Si_5] = 3[Al_5Si_7] + 4Si$
492 Phlogopite Chabazite

493 3) $5[Al_6Si_6] + 12Si = 6[Al_5Si_7]$
494 Haüyne Chabazite

495 4) $5[AlSi] + 2Si = [Al_5Si_7]$
496 Nepheline Chabazite

497 5) $4[AlSi_2] + [Al_6Si_6] = 2[Al_5Si_7]$
498 Leucite Haüyne Chabazite

499 6) $2[AlSi_2] + 3[AlSi] = [Al_5Si_7]$
500 Leucite Nepheline Chabazite

501 Leucite and phlogopite reactions (1) and (2) result in a silica excess, and nepheline and haüyne
502 reactions (3) and (4) consume silica. From the full compositions of chabazite (and phillipsite) in
503 both the *Vallerano* and *Tufo Lionato* samples (Supplementary 2, Table S2.1), it is clear that the
504 reactants included a phase or phases rich in Al and in M^{2+} cations in addition to the alkalis. In all
505 the equations, further Ca and Sr are required for chabazite. The simplest scenario that fulfils
506 these key conditions for the available pool of reactants is a leucite-to-haüyne ratio close to 4:1

(reaction 5), or a leucite-to-nepheline ratio of 2:3 (reaction 6), and/or the presence of an equivalent glass of 'bulk groundmass' composition as hypothesized for the present case study. The results are consistent with a role for magmatic crystal fractionation in providing a significant contribution to the composition of the chabazite alteration product.

When a 5% margin of error (reactants versus products, Supplementary 1, Figure S1) is applied to our case study evidence, the *Tufo Lionato* chabazite compositions remain anomalous and therefore suggestive of a precursor glass derived from a more evolved melt, as illustrated in Figure**s** 5 and 6 and in the reactions above. Nevertheless, the reported scarce fiammae with higher SiO_2/Al_2O_3 ratios (Figure 6) suggest heterogeneity of juvenile components in the *Tufo Lionato* deposit. Collectively, the data indicate that more than one explosively erupted melt composition might reasonably be expected from a complex magma chamber (Cashman and Giordano, 2014).

Overall, the findings in this test-case study suggest that it is possible to achieve a good match of modelled versus analyzed compositions (natural and experimental), and that the model-extrapolated melt composition based on the SiO_2/Al_2O_3 ratio in zeolitic proxy-glass broadly approximates the composition of a melt phase that was assumed to be fractionating until explosive eruption. The melt compositions in our case study have not previously been accessible or recognized. Resolving uncertainties relating to the model input data (mixed volatile concentrations and their impact on magmatic phase relationships especially) will be important for achieving higher precision outputs.

Limitations

The most difficult parameters to constrain in this system are the concentrations of mixed volatiles to use for the model input data (i.e. the 'starting conditions'), because studies of volatile

contents of melt inclusions and other surviving glasses come with inherent issues of representation and interpretation (e.g. post-entrapment resetting, Preece et al., 2014). Mineral/melt/volatile equilibria for mixed-volatile bearing magmatic phases (e.g., F, Cl and S in apatite, mica and sodalite-group minerals) are helpful for defining the system where they are present in the deposits, but they do not provide information on melt H_2O-CO_2 and they could not be modelled in *Rhyolite-MELTS* of the present study (Gualda et al., 2012). The mixed volatile budget of magmas, C-O-H-S-Cl, is considered in numerous studies (e.g. Scaillet and Pichavant, 2005; Iacono-Marziano et al., 2012; Lesne et al., 2011; Vetere et al., 2014; Webster et al., 2014; Lesne et al., 2015; Balassone et al., 2016; and Fiege et al., 2015). However, it is widely understood that H_2O and CO_2 are the dominant phases of magmatic volatiles, and a plethora of melt solubility studies have recently highlighted that alkaline melts may reach solubilities exceeding 9 wt% H_2O (Behrens et al., 2009; Shishkina et al., 2014; Fanara et al., 2015) and solubilities of 4.5 wt% CO_2 at 300 MPa for high K/Na melts (Morizet et al., 2014). Redox state indicators for magmas applicable to the high-K Italian region are evident from several studies (Markl et al., 2010; Morizet et al.,2014; Baudouin and Parat, 2015; and Lesne et al., 2015). Future modelling studies should at least be able to account for two species of carbon, CO_2 and CO_3^{2-}, employing the additional feature of H_2O-CO_2 vapor saturation equilibria available now in a recent model up-grade (Ghiorso and Gualda, 2015). Nevertheless, in the current study where H_2O saturation is repressed and solubility is assessed through comparison with CO_2-free experimental data for ultra-potassic melts, remarkable success has been demonstrated in reproducing mineral compositions known from the natural dataset.

Pressure was fixed at 300 MPa for the modelling exercise in this study, probably representing the deeper end-member of the shallow crustal reservoir, but by definition, the last

553 stages of crystallization of the *Vallerano* lava must have been at surface pressure (0.1 MPa).
554 Nevertheless, where pressure or other input parameters cannot be fully constrained, opportunities
555 remain for bracketing different model variables to examine trends in the system, as has been
556 demonstrated in the present study for the broad relationships between crystallization, H_2O and
557 viscosity (Figure 5b).

558 **Summary**

559 This new application of geochemical data combined with magmatic modelling can uniquely
560 deliver the reconstruction of pre-explosion residual melts for alkaline-mafic pyroclastic deposits.
561 Key lines of evidence in the case of Colli Albani were: (a) lava-tuff geochemical equivalence;
562 (b) a fractional crystallization effect on SiO_2/Al_2O_3; (c) model-system validation by experimental
563 and observed mineralogy; (d) alteration validation by reaction mass balance and independent
564 compositional and stratigraphic reference data; and (e) fractional crystallization and zeolitization
565 effects on the distinctive geochemical pathway of Sr. Successful applications require that the
566 controls on SiO_2/Al_2O_3 in both the magmatic and alteration systems are reasonably understood
567 and validated using benchmark reference data (natural, experimental and modelled). For the
568 Villa Senni caldera-forming eruption, our evidence is indicative of the presence of a more
569 evolved melt fraction (deposited as abundant fine ash) than has previously been understood, with
570 geochemical and physical characteristics predicted from magmatic modelling at the point of
571 quench (explosive eruption).

572

573 **Implications**

574 The presence of a more evolved melt fraction of significant quantity existing at depth
575 immediately prior to the major, caldera-forming eruption of our case study, carries implications

for reappraisal of pre-eruptive conditions, because of new predictions about the melt characteristics. These characteristics would have been different to those previously understood, thereby influencing important inferences about the mechanisms that affected the style of eruption. If replicated across the volcanic stratigraphy, similar patterns of melt evolution prior to other explosive eruptions could therefore contribute further understanding to studies of eruption triggers. Another volcanological implication is that the findings support the notion of complex magma chambers, from which more than one melt fraction can be erupted.

The new approach to accessing pre-eruptive conditions as described here has the potential to serve several other development applications of fundamental importance to volcanology and geochemistry. For example, it could test melt-mush-viscosity hypotheses against deposit characteristics. For mineralogy and crystallography, the case study data have shown how both magmatic and hydrothermal phase relationships have contributed to the unusually high concentrations of Sr in chabazite, with implications also for the behaviors and potential concentration of trace elements such as the rare earth elements.

Wider use of the application will be most successful for magmatic fractionating systems that exhibit significant and unambiguous change in melt SiO_2/Al_2O_3 on cooling, and that are supported by well-constrained phase relationships. Feldspar-absent systems are therefore strongly indicated. Although fresh glass can and should be used, the most 'added value' of the application will be where glass is absent (altered) and where the first formed zeolites constitute a major proportion of the deposits. Compositions of very low SiO_2/Al_2O_3 zeolite proxy-glass similar to those of our *Tufo Lionato* case study are noted worldwide (Supplementary 2, Table S2.1, and Deer et al., 2004) and might therefore be suggestive of similar processes of formation involving quantifiable magmatic fractionation.

599

600 **Acknowledgements**

601 Funding sources supporting the development of this work include NERC grant NE/L002418/1
602 (LC and D. Polya, Manchester University), the Erasmus Staff Training program (LC), a Junior
603 Research Fellowship (Christ's College Cambridge, MS), Indiana University (Bloomington) (DB,
604 LC), and the University of Milan (DG, LC). Field assistance and discussions with S. Conticelli
605 (University of Florence) and several other members of the CARG team (Colli Albani Research
606 Group), plus technical assistance with the microprobe analyses (A. Risplendente and J.
607 Charnock), and loan of thin sections (G. Vignaroli and L. Melluso), are gratefully acknowledged.
608 LC wishes to thank A. Dyer, C. M. B. Henderson and J. Blundy for open and supportive
609 discussions relevant to this work. An earlier version of the manuscript benefitted from expert
610 consideration and welcome suggestions by the editorial and reviewer teams.

611

612 **References Cited**

613 Ames, L.L., (1961). Cation sieve properties of the open zeolites chabazite, mordenite, erionite
614 and clinoptilolite. American Mineralogist, 46(9-10), 1120-1131.
615 Annen, C., Blundy, J.D., Leuthold, J., and Sparks, R.S.J., (2015). Construction and evolution of
616 igneous bodies: Towards an integrated perspective of crustal magmatism. Lithos, 230,
617 206-221.
618 Avanzinelli, R., Lustrino, M., Mattei, M., Melluso, L., and Conticelli, S., (2009). Potassic and
619 ultrapotassic magmatism in the circum-Tyrrhenian region: Significance of carbonated
620 pelitic vs. pelitic sediment recycling at destructive plate margins. Lithos, 113(1-2), 213-
621 227.

622 Avanzinelli, R., Cioni, R., Conticelli, S., Giordano, G., Isaia, R., Mattei, M., Melluso, L.,
623 Sulpizio and R., (2017). The Vesuvius and the other volcanoes of Central Italy.
624 Geological Field Trips, 9(1.1), 158 p.
625 Balassone, G., Bellatreccia, F., Ottolini, L., Mormone, A., Petti, C., Ghiara, M.R., Altomare, A.,
626 Saviano, M., Rizzi, R., and D'Orazio, L., (2016). Sodalite-group minerals from Somma-
627 Vesuvius volcano (Naples, Italy): a combined EPMA, SIMS and FTIR crystal chemical
628 study. The Canadian Mineralogist, 54, 583-604.
629 Baudouin, C. and Parat, F., (2015). Role of volatiles (S, Cl, H_2O) and silica activity on the
630 crystallization of haüyne and nosean in phonolitic magmas (Eifel, Germany and Saghro,
631 Morocco). American Mineralogist, 100(10), 2308-2322.
632 Behrens, H., Misiti, V., Freda, C., Vetere, F., Botcharnikov, R.E., and Scarlato, P., (2009).
633 Solubility of H_2O and CO_2 in ultrapotassic melts at 1200 and 1250 degrees C and
634 pressure from 50 to 500 MPa. American Mineralogist, 94(1), 105-120.
635 Bish, D.L. and Ming, D.W., Eds., (2001). Natural Zeolites: Occurrence, Properties, Applications.
636 Reviews in Mineralogy & Geochemistry, 45, Mineralogical Society of America and
637 Geochemical Society, Washington DC, 654 p.
638 Bish, D.L. and Post, J.E., (1993). Quantitative mineralogical analysis using the Rietveld full-
639 pattern fitting method. American Mineralogist, 78, 932-940.
640 Blundy, J. and Wood, B., (2003). Partitioning of trace elements between crystals and melts.
641 Earth and Planetary Science Letters, 210(3-4), 383-397.
642 Boari, E., Avanzinelli, R., Melluso, L., Giordano, G., Mattei, M., De Benedetti, A.A., Morra, V.,
643 and Conticelli, S., (2009). Isotope geochemistry (Sr-Nd-Pb) and petrogenesis of leucite-
644 bearing volcanic rocks from "Colli Albani" volcano, Roman Magmatic Province, Central

645 Italy: inferences on volcano evolution and magma genesis. Bulletin of Volcanology,
646 71(9), 977-1005.
647 Broxton, D.E., Bish, D.L., and Warren, R.G., (1987). Distribution and chemistry of diagenetic
648 minerals at Yucca Mountain, Nye County, Nevada. Clays and Clay Minerals, 35(2), 89-
649 110.
650 Campbell, L.S., Charnock, J., Dyer, A., Hillier, S., Chenery, S., Stoppa, F., Henderson, C.M.B.,
651 Walcott, R., and Rumsey, M., (2016). Determination of zeolite-group mineral
652 compositions by electron probe microanalysis. Mineralogical Magazine, 80(5), 781-807.
653 Campbell, L.S., Dyer, A., Williams, C., and Lythgoe, P.R., (2012). The masquerade of alkaline-
654 carbonatitic tuffs by zeolites: a new global pathfinder hypothesis. Mineralium Deposita,
655 47(4), 371-382.
656 Cappelletti, P., Petrosino, P., de Gennaro, M., Colella, A., Graziano, S.F., D'Amore, M.,
657 Mercurio, M., Cerri, G., de Gennaro, R., Rapisardo, G., and Langella, A., (2015). The
658 "Tufo Giallo della Via Tiberina" (Sabatini Volcanic District, Central Italy): a complex
659 system of lithification in a pyroclastic current deposit. Mineralogy and Petrology, 109,
660 85-101.
661 Carapezza, M.L., Barberi, F., Tarchini, L., Ranaldi, M., and Ricci, T., (2010). Volcanic hazards
662 of the Colli Albani. In R. Funiciello and G. Giordano, Eds., Colli Albani Volcano, p. 279-
663 297. Special Publications of IAVCEI.
664 Cashman, K.V. and Giordano, G., (2014). Calderas and magma reservoirs. Journal of
665 Volcanology and Geothermal Research, 288, 28-45.
666 Cashman, K.V., Sparks, R.S.J., and Blundy, J.D., (2017). Vertically extensive and unstable
667 magmatic systems: A unified view of igneous processes. Science, 355(6331).

668 Cavarretta, G. and Lombardi, G., (1990). Origin of sulphur in the Quaternary perpotassic melts
669 of Italy: Evidence from haüyne sulphur isotope data. Chemical Geology, 82, 15-20.
670 Chipera, S.J. and Apps, J.A., (2001). Geochemical stability of natural zeolites. Reviews in
671 Mineralogy and Geochemistry, 45, 117-161.
672 Ciotoli, G., Etiope, G., Florindo, F., Marra, F., Ruggiero, L., and Sauer, P.E., (2013). Sudden
673 deep gas eruption nearby Rome's airport of Fiumicino. Geophysical Research Letters,
674 40(21), 5632-5636.
675 Conticelli, S., Avanzinelli, R., Ammannati, E., and Casalini, M., (2015). The role of carbon from
676 recycled sediments in the origin of ultrapotassic igneous rocks in the Central
677 Mediterranean. Lithos, 232, 174-196.
678 Conticelli, S., Boari, E., Avanzinelli, R., De Benedetti, A.A., Giordano, G., Mattei, M., Melluso,
679 L., and Morra, V., (2010). Geochemistry, isotopes and mineral chemistry of the Colli
680 Albani volcanic rocks: constraints on magma genesis and evolution. In R. Funiciello and
681 G. Giordano, (Eds.) The Colli Albani Volcano, p. 107-139. Special Publications of
682 IAVCEI.
683 Conticelli, S. and Peccerillo, A., (1992). Petrology and geochemistry of potassic and
684 ultrapotassic volcanism in central Italy - petrogenesis and inferences on the evolution of
685 the mantle sources. Lithos, 28(3-6), 221-240.
686 Coombs, D.S., Alberti, A., Armbruster, T., Artioli, G., Colella, C., Galli, E., Grice, J.D., Liebau,
687 F., Mandarino, J.A., Minato, H., Nickel, E.H., Passaglia, E., Peacor, D.R., Quartieri, S.,
688 Rinaldi, R., Ross, M., Sheppard, R.A., Tillmanns, E., and Vezzalini, G. (1997)
689 Recommended nomenclature for zeolite minerals: Report of the Subcommittee on
690 Zeolites of the International Mineralogical Association, Commission on New Mineral

691 and Mineral Names. Canadian Mineralogist, 35, 1571-1606.
692 Cross, J.K., Tomlinson, E.L., Giordano, G., Smith, V.C., De Benedetti, A.A., Roberge, J.,
693 Manning, C.J., Wulf, S., and Menzies, M.A., (2014). High level triggers for explosive
694 mafic volcanism: Albano Maar, Italy. Lithos, 190, 137-153.
695 Dai, S., Ward, C. R., Graham, I. T., French, D., Hower, J. C., Zhao, L., and Wang, X. (2017)
696 Altered volcanic ashes in coal and coal-bearing sequences: A review of their nature and
697 significance. Earth Science Reviews, 174, 44-74.
698 De Benedetti, A.A., Caprilli, E., Rossetti, F., and Giordano, G., (2010). Metamorphic,
699 metasomatic and intrusive xenoliths of the Colli Albani volcano and their significance for
700 the reconstruction of the volcano plumbing system. In: Funiciello, R., Giordano, G.
701 (Eds.) The Colli Albani Volcano, p. 153–176. Special Publication of IAVCEI.
702 Deer, W. A., Howie, R. A., Wise, W. S., and Zussman, J., (2004). Rock-Forming Minerals.
703 Framework Silicates: Silica minerals, feldspathoids and the zeolites. Vol. 4B. The
704 Geological Society, Bath, U.K., 982 p.
705 de'Gennaro, B. and Colella, A., (2003). Ba and Co removal from water by elution through fixed
706 beds of phillipsite- and/or chabazite-rich tuffs. Separation Science and Technology,
707 38(10), 2221-2236.
708 de'Gennaro, M. and Langella, A., (1996). Italian zeolitized rocks of technological interest.
709 Mineralium Deposita, 31(6), 452-472.
710 de'Gennaro, M., Langella, A., Cappelletti, P., and Colella, C., (1999). Hydrothermal conversion
711 of trachytic glass to zeolite. 3. Monocationic model glasses. Clays and Clay Minerals,
712 47(3), 348-357.
713 de'Gennaro, M., Adabbo, M., and Langella, A., (1995). Hypothesis on the genesis of zeolites in

some European volcaniclastic deposits. In D. W. Ming and F. A. Mumpton, Eds., Natural Zeolites '93 Occurrence, Properties, Use, p. 51-67. International Committee on Natural Zeolites, Brockport, New York, USA.

de'Gennaro, M. and Franco, E. (1988). Mineralogy of Italian sedimentary phillipsite and chabazite. In D. Kallo and H. S. Sherry, Eds., Occurrence, Properties and Utilization of Natural Zeolites, p. 87-97. Akademiai Kiado, Budapest.

Downes, H., Kostoula, T., Jones, A.P., Beard, A.D., Thirlwall, M.F., and Bodinier, J.L., (2002). Geochemistry and Sr-Nd isotopic compositions of mantle xenoliths from the Monte Vulture carbonatite-melilitite volcano, central southern Italy. Contributions to Mineralogy and Petrology, 144(1), 78-92.

Dyer, A., (2007). Ion-exchange properties of zeolites and related materials. In: J. Čejka, H. VanBekkum, A. Corma and F. Schüth, Eds., Introduction to Zeolite Science and Practice 3rd Revised Edition. Studies in Surface Science and Catalysis, p. 525-553. Elsevier Science, Amsterdam.

Etame, J., Gerard, M., Suh, C.E., and Bilong, P., (2009). Halloysite neoformation during the weathering of nephelinitic rocks under humid tropical conditions at Mt Etinde, Cameroon. Geoderma, 154(1-2), 59-68.

Etame, J., Suh, C.E., Gerard, M., and Bilong, P., (2012). Phillipsite formation in nephelinitic rocks in response to hydrothermal alteration at Mount Etinde, Cameroon. Chemie Der Erde-Geochemistry, 72(1), 31-37.

Eugster, H.P., (1969). Inorganic bedded cherts from Magadi area Kenya. Contributions to Mineralogy and Petrology, 22(1), 1-31.

Fanara, S., Botcharnikov, R.E., Palladino, D.M., Adams, F., Buddensieck, J., Mulch, A., and

Behrens, H., (2015). Volatiles in magmas related to the Campanian Ignimbrite eruption: Experiments vs. natural findings. American Mineralogist, 100(10), 2284-2297.

Fiege, A., Vetere, F., Iezzi, G., Simon, A., and Holtz, F., (2015). The roles of decompression rate and volatiles (H_2O + Cl +/- CO_2 +/- S) on crystallization in (trachy-) basaltic magma. Chemical Geology, 411, 310-322.

Francalanci, L., Peccerillo, A., and Poli, G., (1987). Partition-coefficients for minerals in potassium-alkaline rocks - data from Roman Province (central Italy). Geochemical Journal, 21(1), 1-10.

Freda, C., Gaeta, M., Misiti, V., Mollo, S., Dolfi, D., and Scarlato, P., (2008). Magma-carbonate interaction: An experimental study on ultrapotassic rocks from Alban Hills (Central Italy). Lithos, 101(3-4), 397-415.

Freda, C., Gaeta, M., Palladino, D.M., and Trigila, R., (1997). The Villa Senni Eruption (Alban Hills, Central Italy): The role of H_2O and CO_2 on the magma chamber evolution and on the eruptive scenario. Journal of Volcanology and Geothermal Research, 78(1-2), 103-120.

Funiciello, R. and Giordano, G., Eds., (2010). The Colli Albani volcano. Special Publications of IAVCEI, No. 3, 392 p. The Geological Society.

Gaeta, M., (1998). Petrogenetic implications of Ba-sanidine in the Lionato Tuff (Colli Albani Volcanic District, Central Italy). Mineralogical Magazine, 62(5), 697-701.

Gaeta, M., Freda, C., Christensen, J.N., Dallai, L., Marra, F., Karner, D.B., and Scarlato, P., (2006). Time-dependent geochemistry of clinopyroxene from the Alban Hills (Central Italy): Clues to the source and evolution of ultrapotassic magmas. Lithos, 86(3-4), 330-346.

760 Gaeta, M., Freda, C., Marra, F., Arienzo, I., Gozzi, F., Jicha, B., and Di Rocco, T., (2016).
761 Paleozoic metasomatism at the origin of Mediterranean ultrapotassic magmas:
762 Constraints from time-dependent geochemistry of Colli Albani volcanic products
763 (Central Italy). Lithos, 244, 151-164.
764 Galli, E. and Loschi-Ghittoni, A.G., (1972). Crystal-chemistry of phillipsites. American
765 Mineralogist, 57(7-8), 1125-1145.
766 Ghiara, M.R. and Petti, C., (1995). Chemical alteration of volcanic glasses and related control by
767 secondary minerals: Experimental studies. Aquatic Geochemistry, 1(4), 329-354.
768 Ghiorso, M.S. and Gualda, G.A.R., (2015). An H_2O-CO_2 mixed fluid saturation model
769 compatible with rhyolite-MELTS. Contributions to Mineralogy and Petrology, 169(53),
770 DOI 10.1007/s00410-015-1141-8.
771 Giampaolo, C., Lo Mastro, S., De Rita, D., and Giordano, G., (2008). Lateral and vertical zeolite
772 grade variations in the Tufo Lionato ignimbrite unit (Colli Albani, Roma, Central Italy).
773 In R.S. Bowman and S.E. Delap, Eds., Zeolite 06: The 7th International Conference of
774 the Occurrence, Properties and Utilization of Natural Zeolites, Socorro, New Mexico, p.
775 119-120.
776 Giordano, D., Russell, J.K., and Dingwell, D.B., (2008). Viscosity of magmatic liquids: A
777 model. Earth and Planetary Science Letters, 271(1-4), 123-134.
778 Giordano, G., De Benedetti, A.A., Bonamico, A., Ramazzotti, P., and Mattei, M., (2014).
779 Incorporating surface indicators of reservoir permeability into reservoir volume
780 calculations: Application to the Colli Albani caldera and the Central Italy Geothermal
781 Province. Earth-Science Reviews, 128, 75-92.
782 Giordano, G. and CARG Team, (2010). Stratigraphy, volcano tectonics and evolution of the

783 Colli Albani volcanic field. In R. Funiciello and G. Giordano, Eds., Colli Albani
784 Volcano, p. 43-97. Special Publications of IAVCEI.
785 Gleeson, M.L.M., Stock, M.J., Pyle, D.M., Mather, T.A., Hutchison, W., Yirgu, G., and Wade,
786 J., (2017). Constraining magma storage conditions at a restless volcano in the Main
787 Ethiopian Rift using phase equilibria models. Journal of Volcanology and Geothermal
788 Research, 337, 44-61.
789 Gottardi, G., (1989). The genesis of zeolites. European Journal of Mineralogy, 1(4), 479-487.
790 Gozzi, F., Gaeta, M., Freda, C., Mollo, S., Di Rocco, T., Marra, F., Dallai, L., and Pack, A.,
791 (2014). Primary magmatic calcite reveals origin from crustal carbonate. Lithos, 190, 191-
792 203.
793 Gualda, G.A.R., Ghiorso, M.S., Lemons, R.V., and Carley, T.L., (2012). Rhyolite-MELTS: a
794 modified calibration of MELTS optimized for silica-rich, fluid-bearing magmatic
795 systems. Journal of Petrology, 53(5), 875-890.
796 Hay, R.L., (1964). Phillipsite of saline lakes and soils. American Mineralogist, 49(9-1), 1366-
797 1387.
798 Hay, R.L. and Sheppard, R.A., (2001). Occurrence of zeolites in sedimentary rocks: An
799 overview. Reviews in Mineralogy & Geochemistry, 45, 217-234.
800 Henderson, C.M.B., Richardson, F.R., and Charnock, J.M., (2012). The Highwood Mountains
801 potassic igneous province, Montana: mineral fractionation trends and magmatic processes
802 revisited. Mineralogical Magazine, 76(4), 1005-1051.
803 Hill, E., Wood, B.J., and Blundy, J.D., (2000). The effect of Ca-Tschermaks component on trace
804 element partitioning between clinopyroxene and silicate melt. Lithos, 53(3-4), 203-215.
805 Iacono-Marziano, G., Morizet, Y., Le Trong, E., and Gaillard, F., (2012). New experimental data

and semi-empirical parameterization of H_2O-CO_2 solubility in mafic melts. Geochimica et Cosmochimica Acta, 97, 1-23.

Karner, D.B., Marra, F., and Renne, P.R., (2001). The history of the Monti Sabatini and Alban Hills volcanoes: groundwork for assessing volcanic-tectonic hazards for Rome. Journal of Volcanology and Geothermal Research, 107(1), 185-219.

Langella, A., Bish, D.L., Cappelletti, P., Cerri, G., Colella, A., de Gennaro, R., Graziano, S.F., Perrotta, A., Scarpati, C., and de Gennaro, M., (2013). New insights into the mineralogical facies distribution of Campanian Ignimbrite, a relevant Italian industrial material. Applied Clay Science, 72, 55-73.

Langella, A., Cappelletti, P., and de'Gennaro, R., (2001). Zeolites in closed hydrologic systems. Reviews in Mineralogy & Geochemistry, 45, 235-260.

Lesne, P., Scaillet, B., and Pichavant, M., (2015). The solubility of sulfur in hydrous basaltic melts. Chemical Geology, 418, 104-116.

Lesne, P., Scaillet, B., Pichavant, M., and Beny, J.-M., (2011). The carbon dioxide solubility in alkali basalts: an experimental study. Contributions to Mineralogy and Petrology, 162(1), 153-168.

Markl, G., Marks, M.A.W., and Frost, B.R., (2010). On the controls of oxygen fugacity in the generation and crystallization of peralkaline melts. Journal of Petrology, 51(9), 1831-1847.

Marra, F., Karner, D.B., Freda, C., Gaeta, M., and Renne, P., (2009). Large mafic eruptions at Alban Hills Volcanic District (Central Italy): Chronostratigraphy, petrography and eruptive behavior. Journal of Volcanology and Geothermal Research, 179(3-4), 217-232.

Mattei, M., Conticelli, S., and Giordano, G., (2010). The Tyrrhenian margin geological setting:

from the Apennine orogeny to the K-rich volcanism. In R. Funiciello and G. Giordano, Eds., The Colli Albani Volcano, p. 7-27. Special Publications of IAVCEI.

Mollo, S., Blundy, J.D., Iezzi, G., Scarlato, P., and Langone, A., (2013). The partitioning of trace elements between clinopyroxene and trachybasaltic melt during rapid cooling and crystal growth. Contributions to Mineralogy and Petrology, 166(6), 1633-1654.

Mollo, S., Forni, F., Bachmann, O., Blundy, J.D., De Astis, G., and Scarlato, P., (2016). Trace element partitioning between clinopyroxene and trachy-phonolitic melts: A case study from the Campanian Ignimbrite (Campi Flegrei, Italy). Lithos, 252, 160-172.

Morimoto, N., (1989). Nomenclature of pyroxenes. Canadian Mineralogist, 27, 143-156.

Morizet, Y., Paris, M., Gaillard, F., and Scaillet, B., (2014). Carbon dioxide in silica-undersaturated melt. Part I: The effect of mixed alkalis (K and Na) on CO_2 solubility and speciation. Geochimica et Cosmochimica Acta, 141, 45-61.

Palladino, D.M., Gaeta, M., and Marra, F., (2001). A large K-foiditic hydromagmatic eruption from the early activity of the Alban Hills Volcanic District, Italy. Bulletin of Volcanology, 63(5), 345-359.

Passaglia, E., (1970). Crystal chemistry of chabazites. American Mineralogist, 55(7-8), 1278-1301.

Passaglia.E. and Vezzalini, G., (1985). Crystal chemistry of diagenetic zeolites in volcanoclastic deposits of Italy. Contributions to Mineralogy and Petrology, 90, 190-198.

Passaglia, E., Vezzalini, G., and Carnevali, R., (1990). Diagenetic chabazites and phillipsites in Italy - crystal-chemistry and genesis. European Journal of Mineralogy, 2(6), 827-839.

Preece, K., Gertisser, R., Barclay, J., Berlo, K., and Herd, R.A., (2014). Pre- and syn-eruptive degassing and crystallisation processes of the 2010 and 2006 eruptions of Merapi

volcano, Indonesia. Contributions to Mineralogy and Petrology, 168(4), 1061.

Scaillet, B., and Pichavant, M., (2005). A model of sulphur solubility for hydrous mafic melts: application to the determination of magmatic fluid compositions of Italian volcanoes. Annals of Geophysics, 48(4-5), 671-698.

Sheppard, R.A. and Gude, A.J., (1968). Distribution and genesis of authigenic silicate minerals in tuffs of Pleistocene Lake Tecopa, Inyo County, California. Geological Survey Professional Paper 597, 38 p.

Shishkina, T.A., Botcharnikov, R.E., Holtz, F., Almeev, R.R., Jazwa, A.M., and Jakubiak, A.A., (2014). Compositional and pressure effects on the solubility of H_2O and CO_2 in mafic melts. Chemical Geology, 388, 112-129.

Stock, M.J., Humphreys, M.C.S., Smith, V.C., Isaia, R., and Pyle, D.M., (2016). Late-stage volatile saturation as a potential trigger for explosive volcanic eruptions. Nature Geoscience, 9(3), 249-U290.

Stoppa, F. and Woolley, A.R., (1997). The Italian carbonatites: Field occurrence, petrology and regional significance. Mineralogy and Petrology, 59(1-2), 43-67.

Surdam, R.C. and Eugster, H.P., (1976). Mineral reactions in sedimentary deposits of Lake Magadi region, Kenya. Geological Society of America Bulletin, 87(12), 1739-1752.

Surdam, R.C. and Parker, R.D., (1972). Authigenic aluminosilicate minerals in tuffaceous rocks of Green River Formation, Wyoming. Geological Society of America Bulletin, 83(3), 689-700.

Trigila, R., Agosta, E., Currado, C., De, Benedetti, A.A., Freda, C., Gaeta, M., Palladino, D.M., and Rosa, C., (1995). Petrology. In R. Trigila, Ed., The Volcano of the Alban Hills. SGS, Rome, Italy, p. 95-165.

875 Vaniman, D.T., Chipera, S.J., Bish, D.L., Carey, J.W., and Levy, S.S., (2001). Quantification of
876 unsaturated-zone alteration and cation exchange in zeolitized tuffs at Yucca Mountain,
877 Nevada, USA. Geochimica et Cosmochimica Acta, 65(20), 3409-3433.
878 Vetere, F., Holtz, F., Behrens, H., Botcharnikov, R.E., and Fanara, S., (2014). The effect of
879 alkalis and polymerization on the solubility of H_2O and CO_2 in alkali-rich silicate melts.
880 Contributions to Mineralogy and Petrology, 167, DOI 10.1007/s00410-014-1014-6.
881 Vignaroli, G., Aldega, L., Balsamo, F., Billi, A., De Benedetti, A.A., De Filippis, L., Giordano,
882 G., and Rossetti, F., (2015). A way to hydrothermal paroxysm, Colli Albani volcano,
883 Italy. Geological Society of America Bulletin, 127(5-6), 672-687.
884 Vinkler, A.P., Cashman, K., Giordano, G., and Groppelli, G., (2012). Evolution of the mafic
885 Villa Senni caldera-forming eruption at Colli Albani volcano, Italy, indicated by textural
886 analysis of juvenile fragments. Journal of Volcanology and Geothermal Research, 235,
887 37-54
888 Watkins, S.D., Giordano, G., Cas, R.A.F., and De Rita, D., (2002). Emplacement processes of
889 the mafic Villa Senni Eruption Unit (VSEU) ignimbrite succession, Colli Albani volcano,
890 Italy. Journal of Volcanology and Geothermal Research, 118(1-2), 173-203.
891 Webster, J.D., Goldoff, B., Sintoni, M.F., Shimizu, N., and De Vivo, B., (2014). C-O-H-Cl-S-F
892 volatile solubilities, partitioning, and mixing in phonolitic-trachytic melts and aqueous-
893 carbonic vapor +/- saline liquid at 200 MPa. Journal of Petrology, 55(11), 2217-2247.
894 Wood, B. J., and R, Trigila, R., (2001). Experimental determination of aluminous
895 clinopyroxene–melt partition coefficients for potassic liquids, with application to the
896 evolution of the Roman province potassic magmas. Chemical Geology, 172(3-4), 213-
897 223.

898

899 **Figure captions**

900 **Figure 1**. Map of Colli Albani modified after Giordano et al. (2010) showing the extent of two
901 major depositional units of the Villa Senni eruption and isopachs of the basal fall-out. Orange
902 represents the pervasively zeolitized *Tufo Lionato* (VSN_1) ignimbrite and pink represents the
903 overlying, co-erupted, non-zeolitized, *Pozzolanelle* (VSN_2) ignimbrite. The locations and
904 samples referred to in the present study are labelled in yellow. Further details of the full volcanic
905 succession can be seen in the geological map and stratigraphic column figures of Boari et al.
906 (2009).

907 **Figure 2.** (a) Petrographic texture of the Tufo Lionato deposit (in plane polarized light), showing
908 at least two types of scoria or glassy pumice 'g', some loose crystal fragments (leucite 'lc',
909 clinopyroxene 'cpx', and the pervasive, zeolitized matrix ('z', interstitial, white). The black
910 scoria particle with irregular vesicle shapes filled with zeolites (top left), is apparently similar to
911 'sc2' of Vinkler et al. (2012). (b) Two different scoria/pumice types are depicted in an X-ray
912 map of Fe. Zeolites were analysed from the vesicles of both types, and from the matrix in
913 between. Two leucite fragments are shown, one unaltered (centre, top). (c,d) Zeolite crystals,
914 likely phillipsite 'ph', and chabazite 'ch', in highly vesicular, yellow pumice.

915 **Figure 3.** X-ray maps for *Tufo Lionato* (Fioranello sample) acquired by conventional WDS
916 electron microprobe (operating conditions detailed in Campbell et al., 2016). High-Al chabazite
917 is seen to represent the devitrified, interstitial fine ash component of the rock, with Sr residing
918 there almost exclusively, too. Note the relative distributions of Sr, Ba and Ca, indicative of a
919 compositional zonation with zeolite mineral growth. The horizontal field of view for each map is
920 436μm.

Figure 4. Ternary representations (after Deer et al., 2004) of chabazite and phillipsite series' zeolites in *Tufo Lionato* (this study), with comparator data from the same deposit (de'Gennaro et al., 1996), and lava-hosted chabazite data from the associated pre-caldera succession of the Colli Albani volcano (Passaglia, 1970). **(a)** $R^{+}R^{++}Si$ representation, where T_{Si} = tetrahedral site occupancy by Si. **(b)** Non-framework cations. The M^{2+} apex constitutes the sum of the divalent cations $(Mg,Ca,Sr,Ba)^{2+}$, but Ca^{2+} is dominant. **(c)** Non-framework cations showing the contribution of Sr^{2+} in relation to other M^{2+} cations and to the sum of the alkalis $(Na,K)^{+}$. Slightly higher proportions of Ca and Na are evident in the Villa Adriana sample (base of the deposit, **4b, 4c**), suggesting a minor influence of external fluids. However, the SiO_2/Al_2O_3 ratio is unaffected (**4a**).

Figure 5. Modelled magmatic system characteristics for the pre-caldera stage, Colli Albani, based on the whole-rock composition of the 460 ka Vallerano lava, 300 MPa (Boari et al., 2009) and fO_2 = NNO (Freda et al., 2008). **(a)** Modelled mineralogy and crystallization sequence (see also, Table 3). The evolving SiO_2/Al_2O_3 of the residual melt phase is shown in red. For the Villa Senni eruption, the 'proxy-glass' chabazite signature from the fine ash matrix of the *Tufo Lionato* (VSN) deposit is 2.05 (SiO_2/Al_2O_3). It is considered to represent evidence of a highly fractionated melt phase, quenched on explosive eruption, then zeolitized. **(b)** Modelled evolution of melt-H_2O based on two different starting concentrations (2 and 4 wt% H_2O) and corresponding melt viscosities. The viscosity of a dry melt is included for comparison.

Figure 6. Total alkalis versus silica (TAS) representation of the modelled, fractionating residual melt as it evolves from the start composition (1210°C) towards the lowest temperature that was modelled (789°C), in context of known compositions of natural glasses from *Tufo Lionato*. The modelled melt trajectory passes through the cluster of analyzed, natural compositions, providing

independent validation of our new application. As a further test, the natural glasses were 'reconstructed' on the basis of their SiO_2/Al_2O_3 ratios and re-plotted as TAS representations (i.e. SiO_2 alone). They plot close to their non-reconstructed counterparts, thereby providing further confidence in our approach. Note that melt-H_2O saturation is suppressed, so there is some uncertainty in the lower temperature range of the modelled trajectory of the residual melt.

Figure 7. Compositional trends in modelled clinopyroxene during fractional crystallization (modelled from the Vallerano reference-lava, this study) compared with experimental data for the Villa Senni eruption (1050°C, Freda et al., 2008). The temperature of 1044 °C for the reconstructed melt (proxy glass SiO_2/Al_2O_3 signature, this study) predicts the clinopyroxene composition that would have been crystallizing immediately prior to eruption (vertical, gray bar). The composition is close to that produced in the experiments of Freda et al. (2008) and also to theoretical and natural clinopyroxenes of other studies (Table 4).

Supplementary 1, Figure S1. SiO_2/Al_2O_3 for reactants versus zeolite mineral products. For the low-silica Italian alkaline volcanic deposits, free silica (an SiO_2 phase) is absent in the zeolite-dominant alteration assemblages, but minor smectite is commonly observed. In the highest range of SiO_2/Al_2O_3, greater departure from a perfect correlation is attributed to prolonged interaction with external fluids in an open-system (Broxton et al., 1987, Vaniman et al., 2001). The specified mineral reactant in one study was nepheline (Henderson et al., 2012). Data sources are listed in Supplementary 1, Table S1.1.

Supplementary 1, Figure S2. X-ray maps for *Tufo Lionato* (Villa Adriana sample) acquired by conventional WDS electron microprobe (operating conditions detailed in Campbell et al., 2016). High-Al zeolites occupy vesicles in two different scoria types and also represent the the

966 devitrified, interstitial fine ash component of the rock. Sr almost exclusively resides in the
967 zeolites.

968 **Supplementary 1, Figure S3.** Observed (blue) and Rietveld-refined (red) X-ray powder
969 diffraction patterns for *Tufo Lionato* (IT16 Fioranello). Gray curve represents the difference
970 between observed and calculated patterns, and the tic marks at the bottom of the plot represent
971 the possible positions of all reflections for each component. Details of the determined
972 mineralogy are provided in Table 1.

973 **Supplementary 1, Figure S4.** Compositional framework (SiO_2/Al_2O_3 ratio) for different
974 components of the Colli Albani deposits. See Giordano et al. (2010) for stratigraphic
975 abbreviations (VdL, etc.). Rock, mineral and pumice data are from Freda et al. (1997), Gaeta
976 (1998), Palladino et al. (2001), Marra et al. (2009), Boari et al. (2009), Conticelli et al. (2010),
977 De Benedetti et al. (2010) and Cross et al. (2014), and zeolite data are from Passaglia (1970),
978 Galli and Loschi Ghittoni (1972), Passaglia and Vezzalini (1985), and this study. The dashed-
979 oval represents the SiO_2/Al_2O_3 composition of a profuse, hypothetical former glass that was
980 erupted during the Villa Senni caldera-forming event, as determined in this study.

981

982 **SUPPLEMENTARY FILES:**

983 Supplementary-1 is a *.docx file with four additional figures, one table and references.

984 Supplementary-2 is a *.xls file with tables.

985

986 **TABLES:**

Table 1. Rietvelt-refined weight percentages and unit cell parameters for the mineral constituents of Tufo Lionato.

Parameters	Dioctahedral Smectite*	Phillipsite	Chabazite	Leucite	Analcime	Phlogopite 1M Mica	Diopside	Nepheline
Unit-cell Volume (Å3)		1013.8(8)	837.60(16)	2351.7(10)	2595(2)	492.1(5)	441.4(7)	729.7(11)
Wt% - Rietveld		22(1)	42(1)	9(1)	2.3(3)	6.4(6)	8.1(6)	0.8(3)
Unit-cell parameters:								
a (Å)		9.902(2)	9.4493(6)	13.068(2)	13.741(4)	5.326(4)	9.746(9)	9.979(6)
b (Å)		14.286(5)				9.209(5)	8.903(7)	
c (Å)		8.682(4)		13.771(4)		10.167(5)	5.298(4)	8.461(7)
alpha (°)			93.897(4)					
beta (°)		124.37(3)				99.36(6)	106.23(7)	

*Dioctahedral smectite was not quantified but is evidenced by the broad, low-angle signal, the 02ℓ band, and the 06ℓ band near 62°2θ.

Table 2. Representative compositions of zeolite group minerals for Tufo Lionato (VSN), this study, with comparator compositions. Standard deviations are given in brackets after the mean values. See also, Supplementary 2, Table S2.1

	TUFO LIONATO Pervasive zeolites, mostly from the fine matrix and assumed mostly chabazite (see text for justification).											TUFO LIONATO ZEOLITES			
Location / Reference	IT16 Fioranello			IT118 Villa Adriana (Tivoli) - base of the deposit			[a]Imater quarry				Overall	Passaglia and Vezzalini (1985)	Passaglia et al. (1990)	de'Gennaro et al. (1995)	
														Bulk, separated	
Sample	IT16	IT16	**IT16**	IT118	IT118	**IT118**	Imater	Imater	Imater	**Imater**					
Mineral species	Chabazite-K	Chabazite-K		Chabazite-K	Chabazite-Ca		Chabazite-K	Chabazite-Ca	Phillipsite-K			Phillipsite-K	Phillipsite-K	Phillipsite-K	Chabazite-Ca
Analysis label	#24	#34	**Mean of 11 (s.d.)**	103	126	**Mean of 50 (s.d.)**	136	174	167	**Mean of 53 (s.d.)**	**114 analyses (s.d.)**				
SiO_2	44.65	44.98	**45.93 (2.04)**	49.19	49.28	**50.61 (2.73)**	48.46	49.96	45.85	**49.83 (2.01)**	**49.80 (2.69)**	46.34	44.42	44.83	44.54
Al_2O_3	24.01	22.91	**22.37 (1.34)**	23.91	25.06	**24.58 (1.30)**	23.98	25.10	24.77	**24.73 (1.07)**	**24.44 (1.37)**	21.16	22.18	21.86	19.26
Fe_2O_3													0.18	0.28	0.27
MgO	0.48	0.37	**0.43 (0.15)**	0.06		**0.15 (0.14)**		0.13		**0.14 (0.14)**	**0.18 (0.17)**	0.01			0.04
CaO	5.16	5.49	**4.78 (0.74)**	6.70	8.61	**7.77 (0.69)**	6.42	6.40	7.41	**6.78 (0.63)**	**7.02 (1.1)**	6.70	6.80	6.21	6.10
SrO	5.69	2.19	**4.17 (1.08)**		2.87	**1.43 (0.61)**	0.92	5.82	0.49	**3.35 (1.79)**	**2.53 (1.66)**		0.06	0.15	1.86
BaO		0.43	**0.47 (0.27)**	0.87	0.63	**0.55 (0.16)**	0.80		0.43	**0.65 (0.26)**	**0.59 (0.23)**		0.44	0.47	0.21
Na_2O	1.10	1.24	**1.15 (0.22)**	1.58	1.34	**1.33 (0.43)**	0.63	0.54	0.59	**0.67 (0.14)**	**1.01 (0.44)**	0.60	0.52	0.67	0.84
K_2O	5.64	7.56	**6.50 (1.29)**	8.00	4.88	**5.69 (1.28)**	7.82	5.37	8.29	**7.07 (1.42)**	**6.41 (1.49)**	8.20	7.68	8.28	4.77
Cs_2O			**0.15 (0.02)**								**0.15 (0.02)**				
Total	86.73	85.16	**85.11 (2.15)**	90.31	92.67	**91.63 (3.05)**	89.03	93.32	87.83	**91.72 (1.92)**	**91.04 (3.15)**	83.01	82.28	82.75	77.89
H_2O[c]	13.27	14.84	**14.89 (2.15)**	9.69	7.33	**8.37 (3.05)**	10.97	6.68	12.17	**8.28 (1.92)**	**8.96 (3.15)**	16.60	17.90	17.53	22.40
Number of cations on the basis of 24 framework O (chabazite and unspecified) or 32 framework O (phillipsite)															
	24	24	**24**	24	24	**24**	24	24	**32**	**24**	**24**	32	32	32	24
Si	7.285	7.438	**7.58 (0.24)**	7.622	7.466	**7.64 (0.22)**	7.620	7.557	9.799	**7.60 (0.19)**	**7.62 (0.21)**	10.350	10.070	10.140	7.920
Al	4.616	4.465	**4.35 (0.27)**	4.366	4.475	**4.38 (0.24)**	4.444	4.474	6.239	**4.45 (0.20)**	**4.41 (0.23)**	5.570	5.926	5.830	4.030
Fe3+													0.031	0.050	0.040
∑ Tet	11.901	11.903	**11.94 (0.10)**	11.988	11.941	**12.02 (0.04)**	12.064	12.031	16.037	**12.05 (0.03)**	**12.03 (0.05)**	15.920	16.027	16.020	11.990
Mg	0.116	0.091	**0.08 (0.04)**	0.014		**0.03 (0.03)**		0.029		**0.03 (0.03)**	**0.04 (0.04)**				0.010
Ca	0.903	0.972	**0.85 (0.13)**	1.112	1.398	**1.26 (0.13)**	1.081	1.037	1.697	**1.11 (0.11)**	**1.15 (0.17)**	1.550	1.652	1.500	1.160
Sr	0.539	0.210	**0.40 (0.11)**		0.252	**0.13 (0.05)**	0.084	0.510	0.060	**0.30 (0.16)**	**0.23 (0.15)**		0.008	0.020	0.190
Ba		0.028	**0.03 (0.02)**	0.053	0.037	**0.03 (0.01)**	0.049		0.036	**0.04 (0.02)**	**0.04 (0.01)**	0.030	0.039	0.040	0.010
Na	0.348	0.397	**0.37 (0.07)**	0.475	0.393	**0.39 (0.12)**	0.192	0.159	0.245	**0.20 (0.04)**	**0.30 (0.13)**	0.250	0.229	0.290	0.290
K	1.174	1.596	**1.37 (0.25)**	1.581	0.943	**1.09 (0.24)**	1.568	1.036	2.260	**1.38 (0.29)**	**1.25 (0.3)**	2.270	2.221	2.390	1.080
Cs			**0.01** ***(<0.005)***								**0.01 (<0.005)**				
∑ EC[b]	3.080	3.294	**3.040 (0.18)**	3.235	3.023	**2.889 (0.15)**	2.975	2.772	4.297	**2.913 (0.19)**	**2.91 (0.18)**	4.100	4.149	4.240	2.740
R =Si/(Si+Al+Fe^{3+})	0.61	0.62	**0.64 (0.02)**	0.64	0.63	**0.64 (0.02)**	0.63	0.63	0.61	**0.63 (0.02)**	**0.63 (0.02)**	0.65	0.63	0.63	0.66
E% (Passaglia 1970)	-0.47	-2.83		-1.07	-5.00		6.08	2.88	2.44			-4.90	1.90	1.03	-1.39
SiO_2/Al_2O_3	1.86	1.96	**2.05 (0.20)**	2.06	1.97	**2.06 (0.17)**	2.02	1.99	1.85	**2.01 (0.15)**	**2.04 (0.16)**	2.19	2.00	2.05	2.31

[a]Imater quarry sample: courtesy of G. Vignaroli, and described in Vignaroli et al. (2014). [b]Extra-framework cations. [c]H_2O by difference (this study).

Summary of operating conditions (after Campbell et al., 2016):

Fioranello sample - Cameca SX100 WDS microprobe (University of Manchester, U.K.), 2nA, 15kV, 20µm defocussed beam.

Villa Adriana and Imater samples - Jeol 8200 Super Probe (University of Milan, Italy), 2nA, 15kV, 20 and 10 µm defocussed beam.

Table 3. Reconstruction of an explosively-erupted melt composition from the SiO_2/Al_2O_3 signature of zeolitic proxy-glass coupled to the SiO_2/Al_2O_3 cooling profile of the modelled residual melt. Modelled using "Rhyolite-MELTS", Gualda et al. (2012).

	Boari et al.(2009)	Boari et al.(2009)	Model - **This study**, Gualda et al. (2012)	Passaglia (1970)	de'Gennaro et al. (1995)	**This study** (average Fioranello zeolite, IT16)	**This study**
	Whole rock (WR)	Whole rock (WR)	**Model INPUT: 'Start' melt**	Chabazite	Phillipsite	**Chabazite 'proxy glass'**	**Model OUTPUT: residual melt**
	"Reference lava" Vallerano VLS 05	Tufo Lionato VSN, CA 32	**'Reference lava' Vallerano VLS 05**	Host: Vallerano lava (No.5)	Tufo Lionato VSN bulk, separated	**Tufo Lionato VSN, pervasive matrix**	**Tufo Lionato VSN, pervasive matrix**
	Analytical data	Analytical data	**Model composition at "Start" (WR)**	Analytical data	Analytical data	**Analytical data (Tables 2 and S2.1)**	**Model-extracted, erupted melt composition**
SiO_2/Al_2O_3	*2.68*		*2.68*	*1.73*	*2.05*	***2.05*** →	***2.05***
Composition (wt%)							
SiO_2	44.0	48.4	44.0	38.85	44.83	45.93	**45.01**
TiO_2	0.74	0.82	0.74				**0.4**
Al_2O_3	16.4	18.3	16.4	22.41	21.86	22.37	**21.93**
Fe_2O_3	5.25	8.46	5.25	0.1	0.28		**0.77**
FeO	3.74		3.74				**1.71**
MnO	0.16	0.25	0.16				**0.37**
MgO	4.67	1.27	4.67	0.06		0.43	**0.74**
CaO	10.6	4.46	10.6	5.25	6.21	4.78	**7.25**
SrO	0.26	0.23		3.78	0.15	4.17	
BaO				0.8	0.47	0.47	
Na_2O	2.75	2.37	2.75	0.78	0.67	1.15	**6.07**
K_2O	8.68	7.15	8.68	5.76	8.28	6.5	**10.52**
P2O5	0.78	0.15	0.78				**0.93**
LOI	2.22	7.59					
H_2O wt%			2	21.38	17.53	14.89	**4.29**
Sum	100.25	99.45	99.77	99.17	100.28	100.69	**99.99**
Physical parameters							
T (°C)			~1200				**1044.30**
P (kbars)			3				**3**
log(10) f O2			(NNO)				**-9.56**
liq mass (gm)							**43.45**
liq rho (gm/cc)							**2.32**
liq vis (log 10 poise)							**1.99**
sol mass (gm)							**1.13**
sol rho (gm/cc)							**2.74**

989

Table 4. Clinopyroxene and nepheline data (oxide wt%): Comparison of modelled compositions (this study - **bold**) with natural, theoretical and experimental compositions (published sources).

	CLINOPYROXENE										NEPHELINE		
	Conticelli et al. (2010) Table 3a Clinopyroxene, Core	Gaeta et al. (2006) Table 2 Clinopyroxene, Phenocryst	**This study** **Clinopyroxene (model data)**	Boari et al.(2009) Table 3 Clinopyroxene, Groundmass	Gaeta et al. (2006) Table 2 Clinopyroxene, Groundmass	Freda et al. (2008) Table 3 Clinopyroxene Table 3 Experimental	Palladino et al. (2001) Table 4 Clinopyroxene Theoretical	Gaeta et al. (2006) Table 2 Clinopyroxene, Scoria	Gaeta et al. (2006) Table 2 Clinopyroxene, Scoria	**This study** **Clinopyroxene (model data)**	Boari et al.(2009) Table 4 Nepheline, Groundmass	Gozzi et al (2014) Nepheline (post-caldera)	**This study** **Nepheline (model data)**
	Vallerano	Vallerano	**Vallerano-model, earliest crystallized**	Vallerano	Vallerano	Lava (308 ka), 1% H_2O, 3% $CaCO_3$	Tufo Lionato VSN (VSEU)	Tufo Lionato VSN (VSEU)	Tufo Lionato VSN (VSEU)	**Vallerano-model, intermediate stage**	Vallerano	Monte delle Faete lava	**Vallerano-partially crystallized**
	Analytical data VLS 07	Analytical data PH3	**Model-extracted, 1169°C**	Analytical data VLS 20	Analytical data GM2	Experimental product 247/29 at 1050°C	Calculated	LFU2	UFU2	**Model-extracted, 1044°C 'at eruption'**	Analytical data VLS 20	Analytical data AH32 ne1	**Model-extracted, first appearance at 839 °C**
SiO_2/Al_2O_3	*14.61*	*16.12*	***10.60***	*4.89*	*4.16*	*4.58*	*4.28*	*5.48*	*7.55*	***3.64***	*1.24*	*1.33*	***1.18***
SiO_2	49.1	50.45	**49.3**	44.4	42.01	45.66	43.43	43.47	46.21	**40.30**	42.10	44.06	**41.33**
TiO_2	0.64	0.51	**0.6**	1.77	2.6	1.22	0.22	1.39	1.06	**4.01**			
Al_2O_3	3.36	3.13	**4.65**	9.08	10.11	9.98	10.15	7.93	6.12	**11.06**	33.90	33.10	**35.06**
Fe_2O_3	4.15		**4.62**	*see below*			9.36			**7.46**	0.78		
FeO	6.14	6.07	**3.01**	9.82	9.85	8.66	2.18	11.61	9.01	**3.88**		0.53	
MnO	0.46			0.07	0.07	0.1		0.34	0.15				
MgO	11.5	14.62	**13.98**	11.4	10.1	10.53	10.6	9.8	12.03	**9.24**			
CaO	23.8	23.94	**24.03**	24	23.51	22.27	23.97	23.62	23.97	**23.85**	0.64	2.04	**2.22**
Na_2O	0.35	0.33	**0.1**	0.18	0.49	0.75	0.06	0.39	0.26	**0.19**	13.70	15.53	**14.01**
K_2O											9.07	4.12	**7.39**
Sum	99.5	99.05	100.29	100.72	98.74	99.17	99.97	98.55	98.81	100.00	100.19	99.38	100.01
Fe_2O_3				*7.89*									
SrO											0.27	0.16	
BaO												0.01	
Physical parameters													
T (°C)			**1169.00**			1050				**1044.3**			**839**
P (kbars)			**3**							**3**			**3**

Table 2. Representative compositions of zeolite group minerals for Tufo Lionato (

Location / Reference	TUFO LIONATO Pervasive zeolites, mostly from the fine matrix an				
	IT16 Fioranello			IT118 Villa Adriana (T the depos	
Sample	IT16	IT16	**IT16**	IT118	IT118
Mineral species	Chabazite-K	Chabazite-K		Chabazite-K	Chabazite-Ca
Analysis label	#24	#34	Mean of 11 (s.d.)	103	126
SiO_2	44.65	44.98	**45.93 (2.04)**	49.19	49.28
Al_2O_3	24.01	22.91	**22.37 (1.34)**	23.91	25.06
Fe_2O_3					
MgO	0.48	0.37	**0.43 (0.15)**	0.06	
CaO	5.16	5.49	**4.78 (0.74)**	6.70	8.61
SrO	5.69	2.19	**4.17 (1.08)**		2.87
BaO		0.43	**0.47 (0.27)**	0.87	0.63
Na_2O	1.10	1.24	**1.15 (0.22)**	1.58	1.34
K_2O	5.64	7.56	**6.50 (1.29)**	8.00	4.88
Cs_2O			**0.15 (0.02)**		
Total	86.73	85.16	**85.11 (2.15)**	90.31	92.67
H_2O[c]	13.27	14.84	**14.89 (2.15)**	9.69	7.33
Number of cations on the basis of 24 framework O (chabazite and unspecified) or 32 framework C					
	24	24	**24**	24	24
Si	7.285	7.438	**7.58 (0.24)**	7.622	7.466
Al	4.616	4.465	**4.35 (0.27)**	4.366	4.475
Fe3+					
∑ Tet	11.901	11.903	**11.94 (0.10)**	11.988	11.941
Mg	0.116	0.091	**0.08 (0.04)**	0.014	
Ca	0.903	0.972	**0.85 (0.13)**	1.112	1.398
Sr	0.539	0.210	**0.40 (0.11)**		0.252
Ba		0.028	**0.03 (0.02)**	0.053	0.037
Na	0.348	0.397	**0.37 (0.07)**	0.475	0.393
K	1.174	1.596	**1.37 (0.25)**	1.581	0.943
Cs			**0.01** ***(<0.005)***		
∑ EC[b]	3.080	3.294	**3.040 (0.18)**	3.235	3.023
R =Si/(Si+Al+Fe^{3+})	0.61	0.62	**0.64 (0.02)**	0.64	0.63
E% (Passaglia 1970)	-0.47	-2.83		-1.07	-5.00
SiO_2/Al_2O_3	1.86	1.96	**2.05 (0.20)**	2.06	1.97

[a]Imater quarry sample: courtesy of G. Vignaroli, and described in Vignaroli et al. (2014). [b]Extra-fra

Summary of operating conditions (after Campbell et al., 2016):

Fioranello sample - Cameca SX100 WDS microprobe (University of Manchester, U.K.), 2nA, 15kV

Villa Adriana and Imater samples - Jeol 8200 Super Probe (University of Milan, Italy), 2nA, 15kV,

VSN), this study, with comparator compositions. Standard deviations are given in brackets

d assumed mostly chabazite (see text for justification).

ivoli) - base of sit	[a]Imater quarry				Overall
IT118	Imater Chabazite-K	Imater Chabazite-Ca	Imater Phillipsite-K	**Imater**	
Mean of 50 (s.d.)	136	174	167	**Mean of 53** (s.d.)	**114 analyses**
50.61 (2.73)	48.46	49.96	45.85	**49.83 (2.01)**	**49.80**
24.58 (1.30)	23.98	25.10	24.77	**24.73 (1.07)**	**24.44**
0.15 (0.14)		0.13		**0.14 (0.14)**	**0.18**
7.77 (0.69)	6.42	6.40	7.41	**6.78 (0.63)**	**7.02**
1.43 (0.61)	0.92	5.82	0.49	**3.35 (1.79)**	**2.53**
0.55 (0.16)	0.80		0.43	**0.65 (0.26)**	**0.59**
1.33 (0.43)	0.63	0.54	0.59	**0.67 (0.14)**	**1.01**
5.69 (1.28)	7.82	5.37	8.29	**7.07 (1.42)**	**6.41**
					0.15
91.63 (3.05)	89.03	93.32	87.83	**91.72 (1.92)**	**91.04**
8.37 (3.05)	10.97	6.68	12.17	**8.28 (1.92)**	**8.96**
) (phillipsite)					
24	24	24	**32**	**24**	**24**
7.64 (0.22)	7.620	7.557	9.799	**7.60 (0.19)**	**7.62**
4.38 (0.24)	4.444	4.474	6.239	**4.45 (0.20)**	**4.41**
12.02 (0.04)	12.064	12.031	16.037	**12.05 (0.03)**	**12.03**
0.03 (0.03)		0.029		**0.03 (0.03)**	**0.04**
1.26 (0.13)	1.081	1.037	1.697	**1.11 (0.11)**	**1.15**
0.13 (0.05)	0.084	0.510	0.060	**0.30 (0.16)**	**0.23**
0.03 (0.01)	0.049		0.036	**0.04 (0.02)**	**0.04**
0.39 (0.12)	0.192	0.159	0.245	**0.20 (0.04)**	**0.30**
1.09 (0.24)	1.568	1.036	2.260	**1.38 (0.29)**	**1.25**
					0.01
2.889 (0.15)	2.975	2.772	4.297	**2.913 (0.19)**	**2.91**
0.64 (0.02)	0.63	0.63	0.61	**0.63 (0.02)**	**0.63**
	6.08	2.88	2.44		
2.06 (0.17)	2.02	1.99	1.85	**2.01 (0.15)**	**2.04**

amework cations. [c]H_2O by difference (this study).

/, 20μm defocussed beam.
20 and 10 μm defocussed beam.

s after the mean values. See also, Supplementary 2, Table S2.1

	TUFO LIONATO ZEOLITES			
	Passaglia and Vezzalini (1985)	Passaglia et al. (1990)	de'Gennaro et al. (1995)	
			Bulk, separated	
	Phillipsite-K	Phillipsite-K	Phillipsite-K	Chabazite-Ca
(s.d.)				
(2.69)	46.34	44.42	44.83	44.54
(1.37)	21.16	22.18	21.86	19.26
		0.18	0.28	0.27
(0.17)	0.01			0.04
(1.1)	6.70	6.80	6.21	6.10
(1.66)		0.06	0.15	1.86
(0.23)		0.44	0.47	0.21
(0.44)	0.60	0.52	0.67	0.84
(1.49)	8.20	7.68	8.28	4.77
(0.02)				
(3.15)	83.01	82.28	82.75	77.89
(3.15)	16.60	17.90	17.53	22.40
	32	32	32	24
(0.21)	10.350	10.070	10.140	7.920
(0.23)	5.570	5.926	5.830	4.030
		0.031	0.050	0.040
(0.05)	15.920	16.027	16.020	11.990
(0.04)				0.010
(0.17)	1.550	1.652	1.500	1.160
(0.15)		0.008	0.020	0.190
(0.01)	0.030	0.039	0.040	0.010
(0.13)	0.250	0.229	0.290	0.290
(0.3)	2.270	2.221	2.390	1.080
(<0.005)				
(0.18)	4.100	4.149	4.240	2.740
(0.02)	0.65	0.63	0.63	0.66
	-4.90	1.90	1.03	-1.39
(0.16)	2.19	2.00	2.05	2.31

Modelled magmatic system
FRACTIONAL CRYSTALLISATION

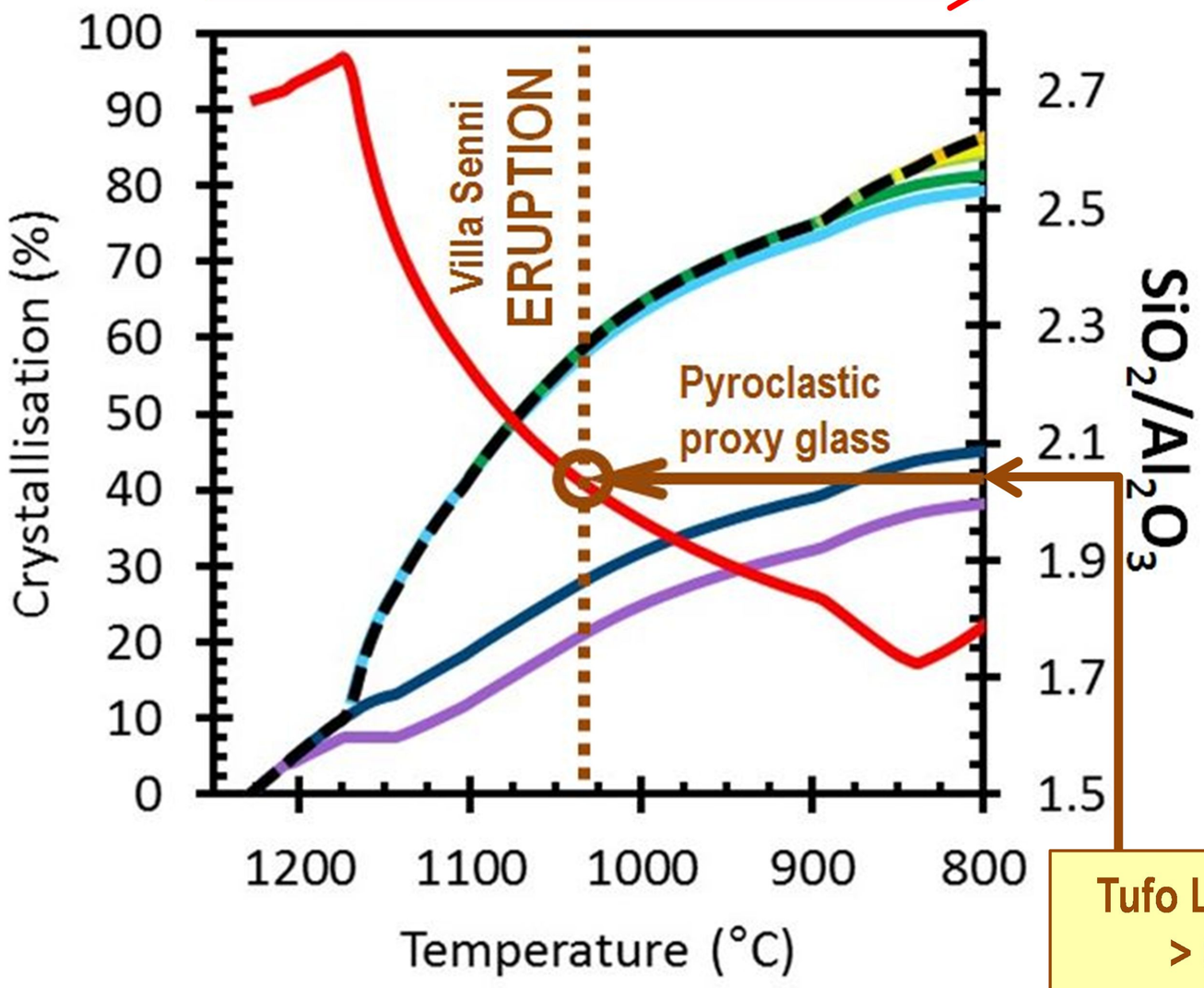

Tufo Lionato:
> 60%
zeolitized

- Leucite
- Spinel
- Clinopyroxene
- Apatite
- Garnet
- Plagioclase
- Nepheline
- Total solids
- SiO_2/Al_2O_3 residual melt

Measured SiO_2/Al_2O_3
→ PROXY GLASS

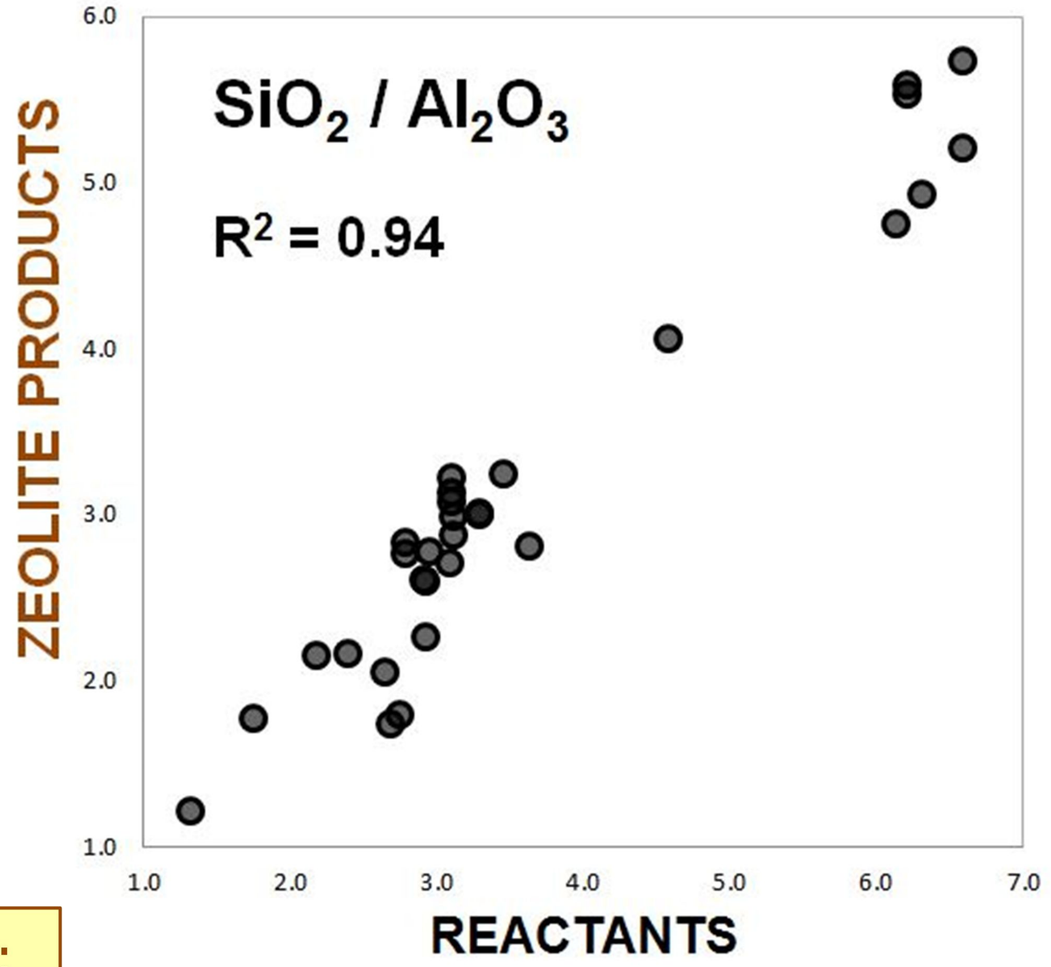

VALIDATION

Natural + experimental assemblages

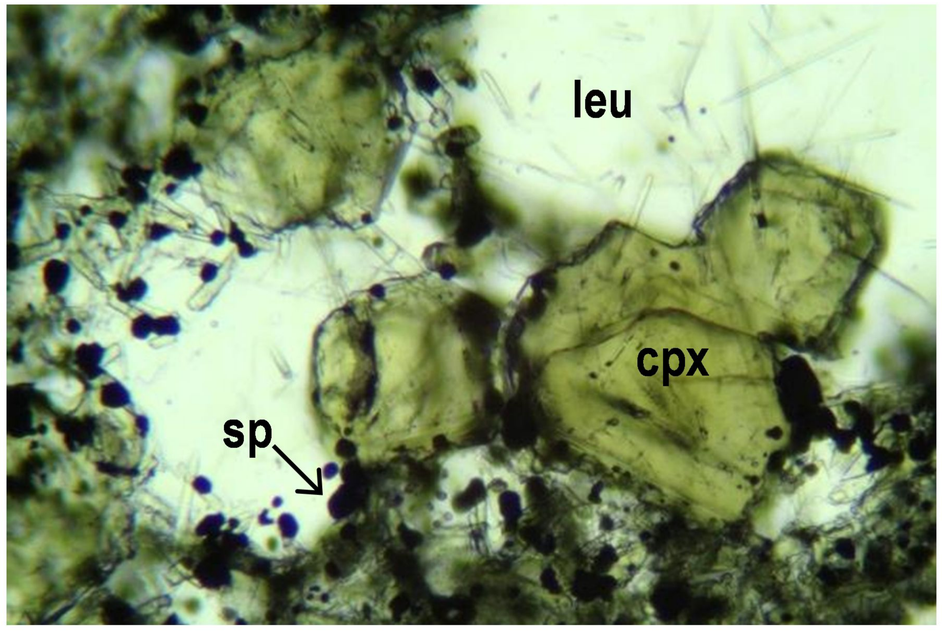

and compositions

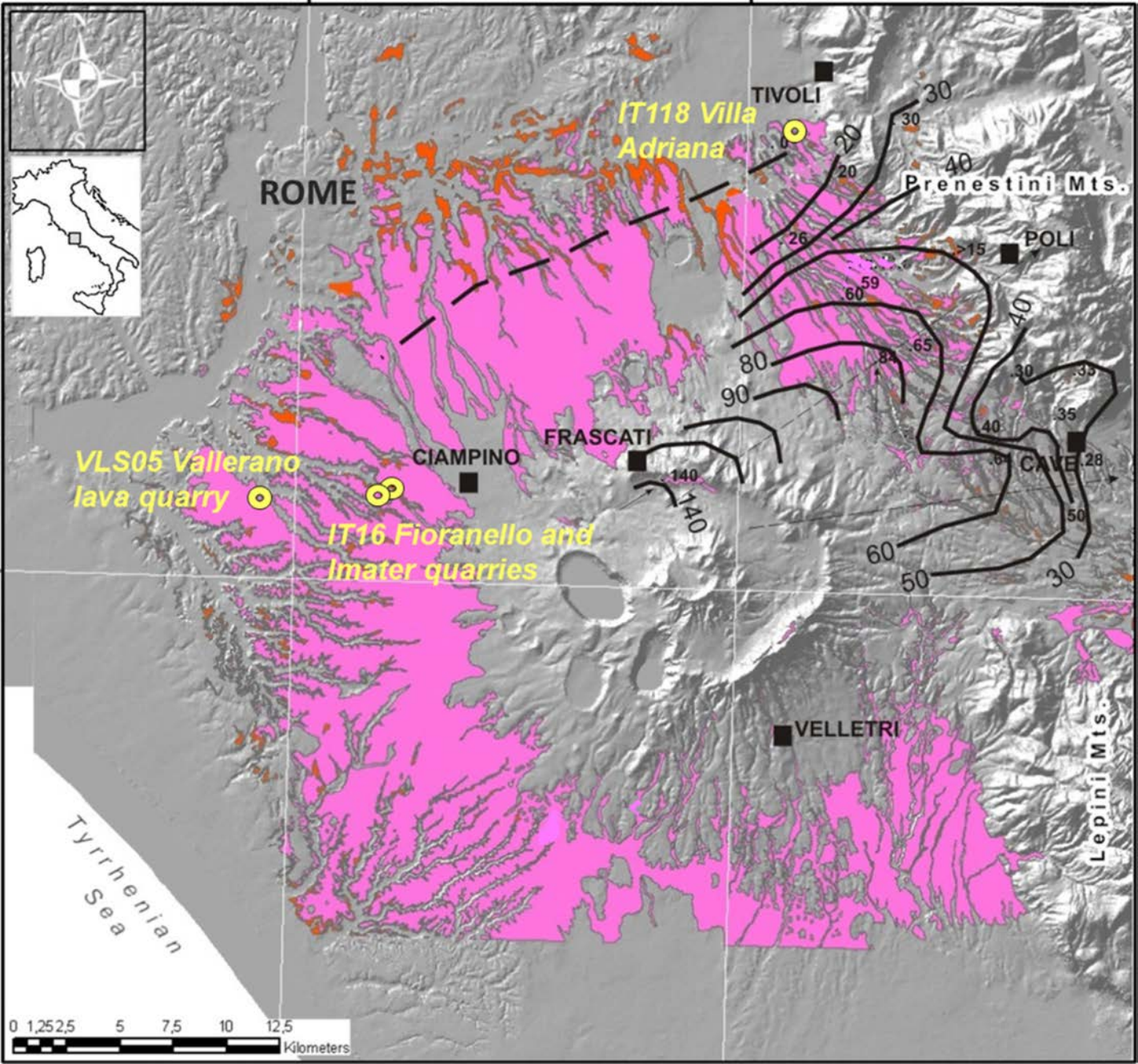
ROME
TIVOLI
IT118 Villa Adriana
Prenestini Mts.
POLI
FRASCATI
CIAMPINO
VLS05 Vallerano lava quarry
IT16 Fioranello and Imater quarries
CAVE
VELLETRI
Lepini Mts.
Tyrrhenian Sea
0 1,25 2,5 5 7,5 10 12,5
Kilometers

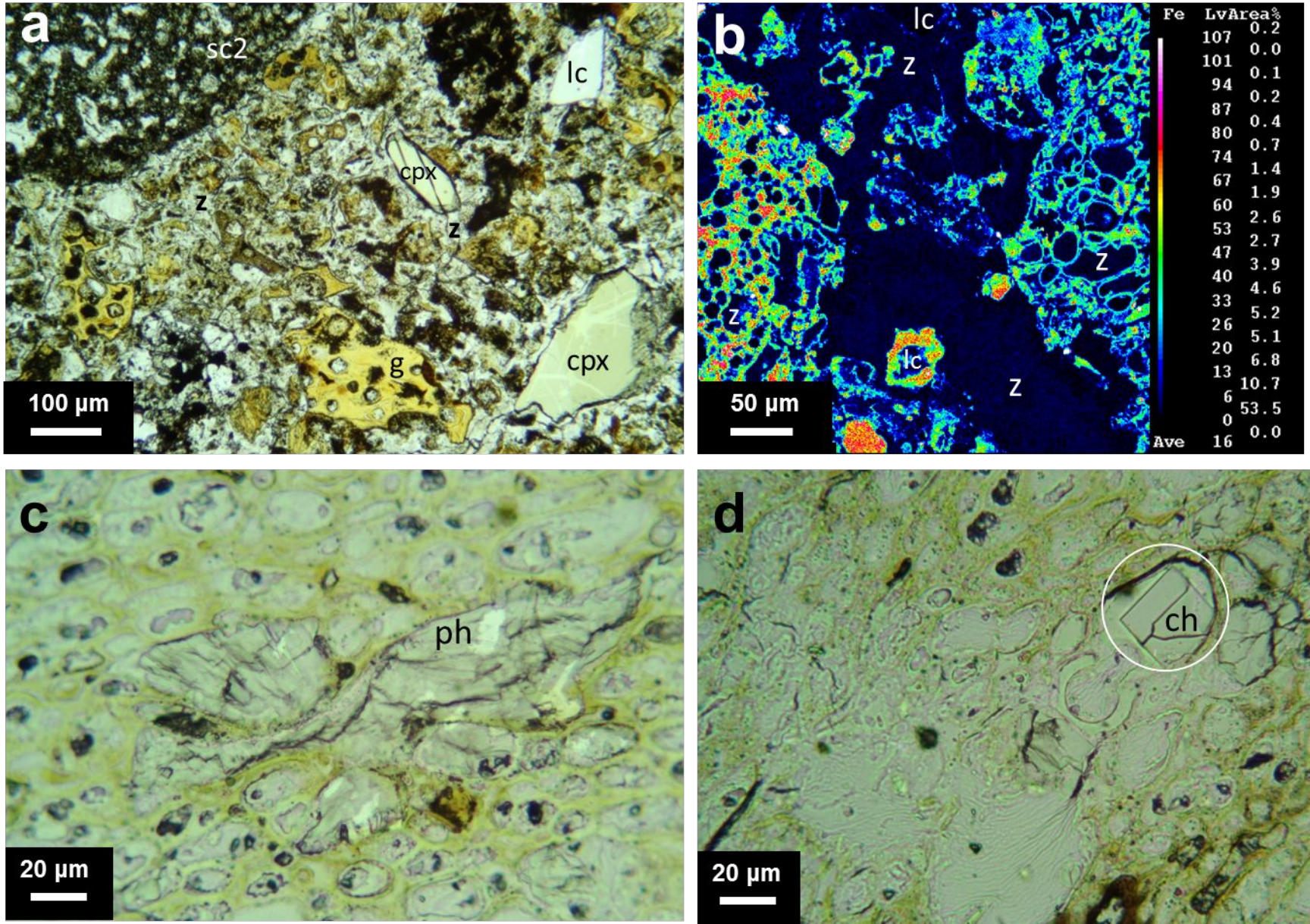
a
sc2
lc
cpx
z
z
g
cpx
100 µm
b
lc
z
z
z
lc
z
50 µm
Fe LvArea%
107 0.2
101 0.0
94 0.1
87 0.2
80 0.4
74 0.7
67 1.4
60 1.9
53 2.6
47 2.7
40 3.9
33 4.6
26 5.2
20 5.1
13 6.8
6 10.7
0 53.5
Ave 16 0.0
c
ph
20 µm
d
ch
20 µm

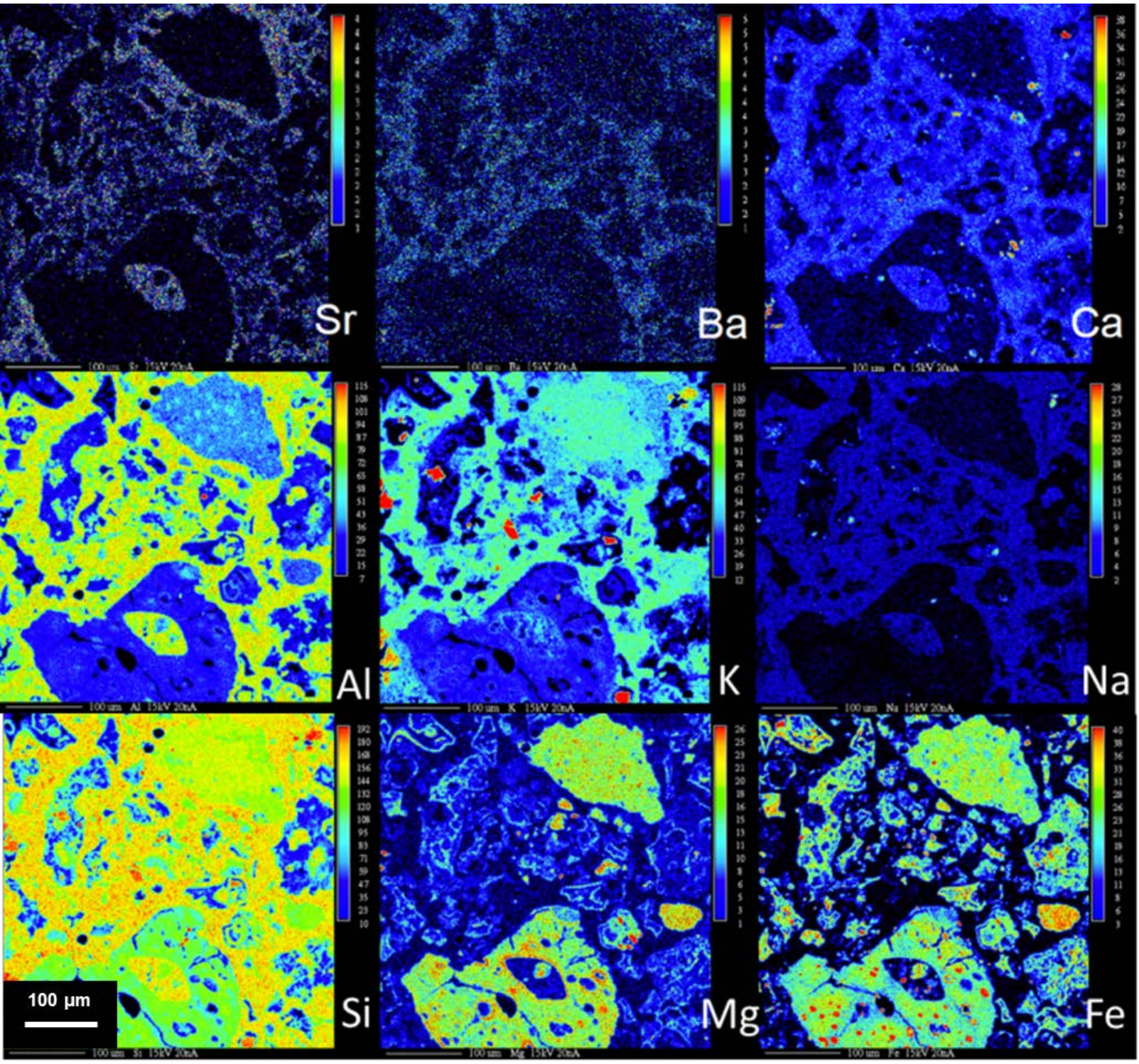
Sr
Ba
Ca
Al
K
Na
Si
Mg
Fe
100 µm

Figure 4a

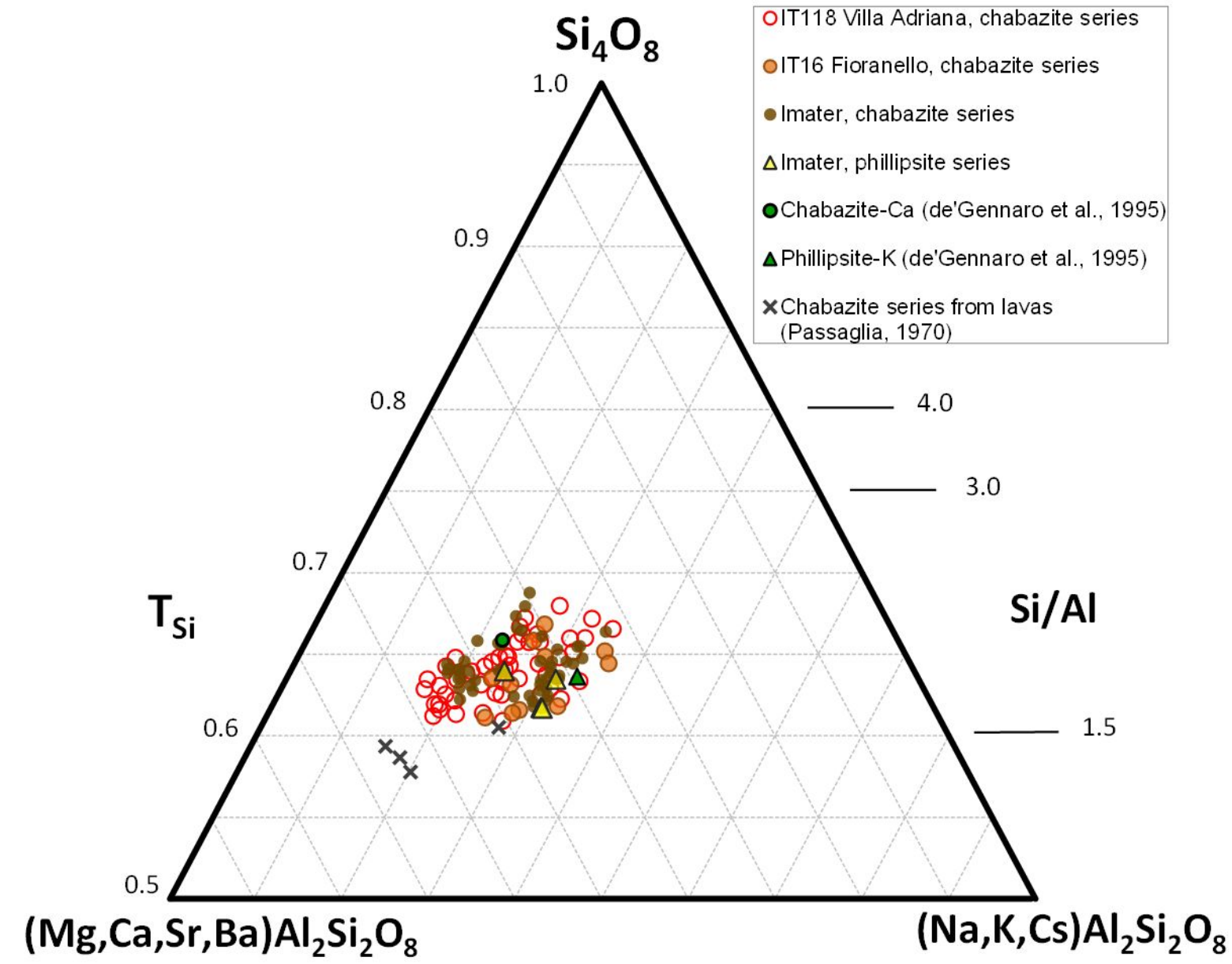
Si4O8
1.0
0.9
0.8
0.7
0.6
0.5
TSi
Si/Al
4.0
3.0
1.5
(Mg,Ca,Sr,Ba)Al2Si2O8
(Na,K,Cs)Al2Si2O8
IT118 Villa Adriana, chabazite series
IT16 Fioranello, chabazite series
Imater, chabazite series
Imater, phillipsite series
Chabazite-Ca (de'Gennaro et al., 1995)
Phillipsite-K (de'Gennaro et al., 1995)
Chabazite series from lavas (Passaglia, 1970)

Figure 4b

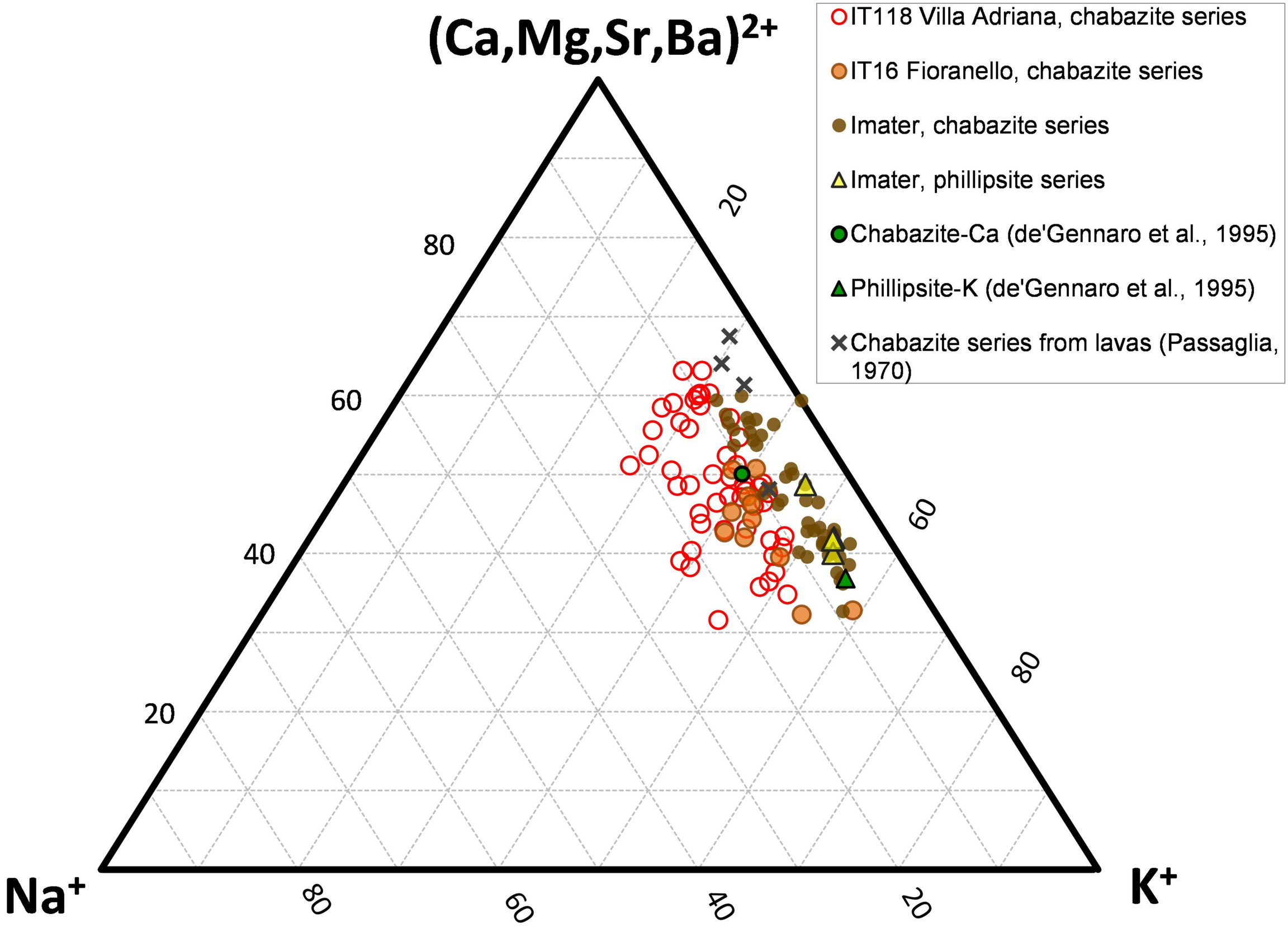
(Ca,Mg,Sr,Ba)2+
Na+
K+
20
40
60
80
IT118 Villa Adriana, chabazite series
IT16 Fioranello, chabazite series
Imater, chabazite series
Imater, phillipsite series
Chabazite-Ca (de'Gennaro et al., 1995)
Phillipsite-K (de'Gennaro et al., 1995)
Chabazite series from lavas (Passaglia, 1970)

Figure 4c

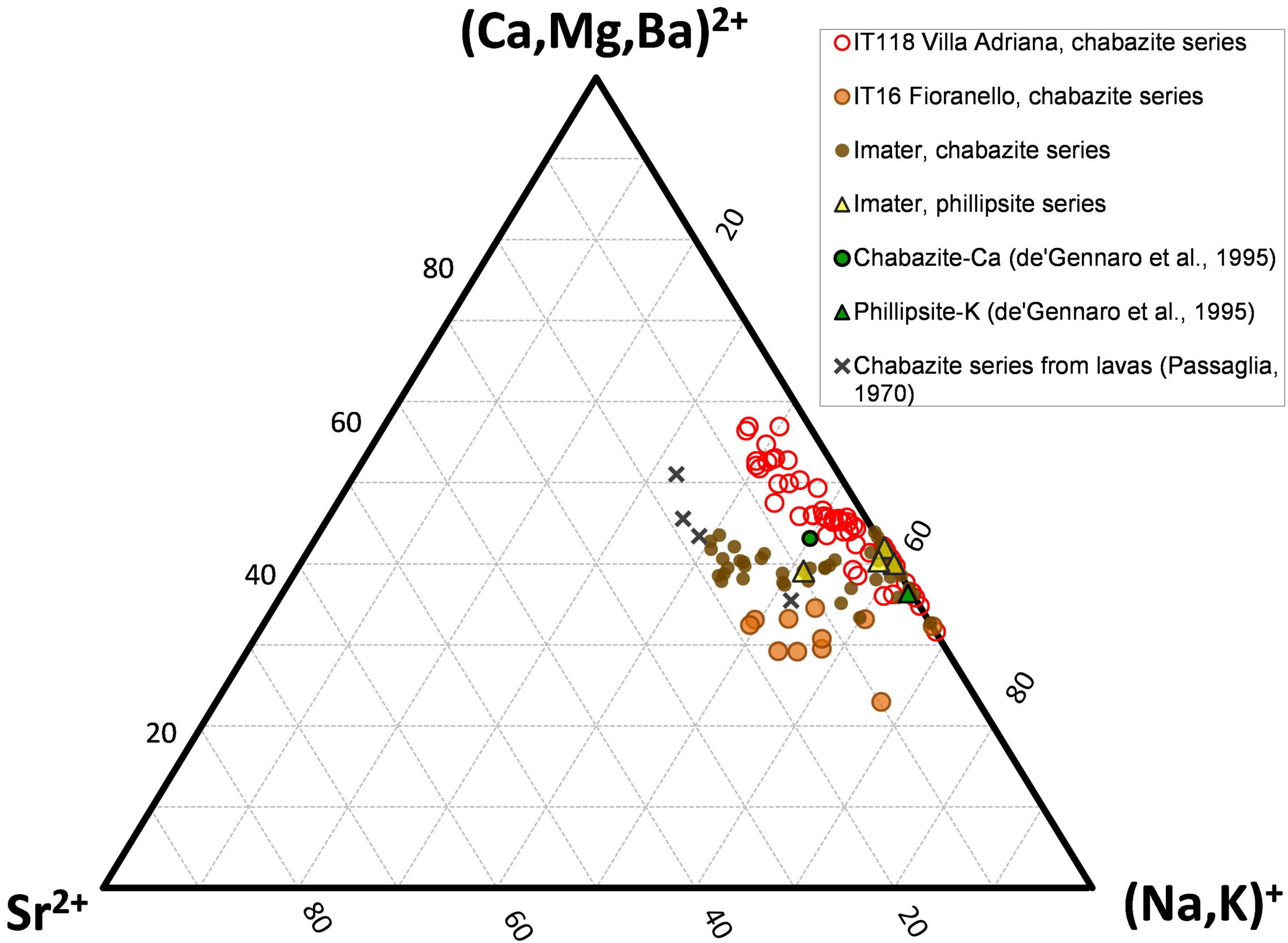
(Ca,Mg,Ba)2+
Sr2+
(Na,K)+
20
40
60
80
IT118 Villa Adriana, chabazite series
IT16 Fioranello, chabazite series
Imater, chabazite series
Imater, phillipsite series
Chabazite-Ca (de'Gennaro et al., 1995)
Phillipsite-K (de'Gennaro et al., 1995)
Chabazite series from lavas (Passaglia, 1970)

Leucite
Spinel
Clinopyroxene
Apatite
Garnet
Plagioclase
Nepheline
Total solids
SiO_2/Al_2O_3 Residual melt

Dissolved H_2O conc. in melt
4 wt% (starting H_2O)
2 wt% (starting H_2O)
Viscosity
4 wt% (starting H_2O)
2 wt% (starting H_2O)
0 wt% (starting H_2O)
H_2O solubility
300 MPa

a
ERUPTION
VSN proxy glass
Crystallisation (%)
SiO_2/Al_2O_3
b
Viscosity (log10 poise)
Melt H_2O (wt%)
Temperature (°C)

Figure 6

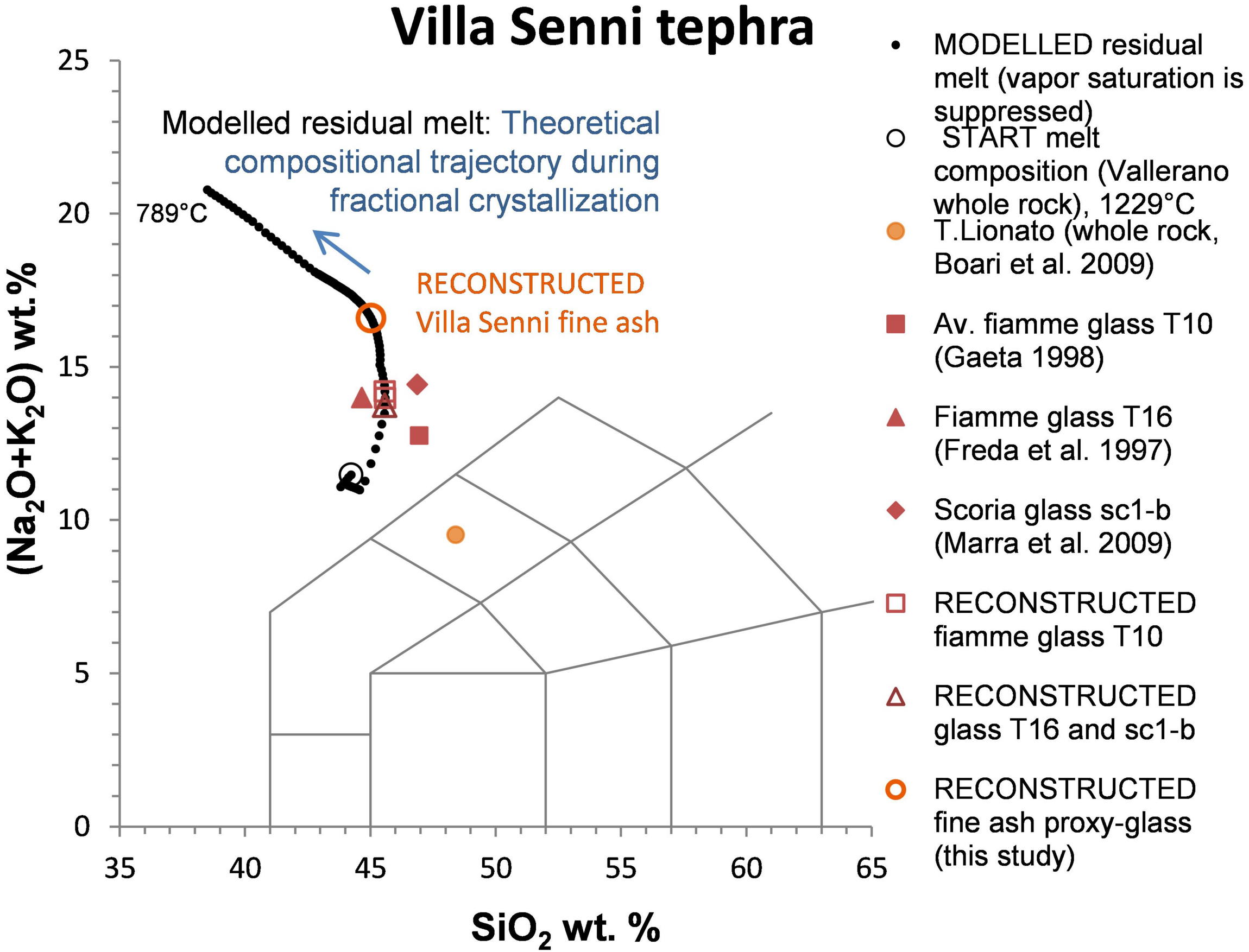
Villa Senni tephra
Modelled residual melt: Theoretical compositional trajectory during fractional crystallization
789°C
RECONSTRUCTED
Villa Senni fine ash
25
20
15
10
5
0
35
40
45
50
55
60
65
(Na2O+K2O) wt.%
SiO2 wt. %
MODELLED residual melt (vapor saturation is suppressed)
START melt composition (Vallerano whole rock), 1229°C
T.Lionato (whole rock, Boari et al. 2009)
Av. fiamme glass T10 (Gaeta 1998)
Fiamme glass T16 (Freda et al. 1997)
Scoria glass sc1-b (Marra et al. 2009)
RECONSTRUCTED fiamme glass T10
RECONSTRUCTED glass T16 and sc1-b
RECONSTRUCTED fine ash proxy-glass (this study)

Figure 7

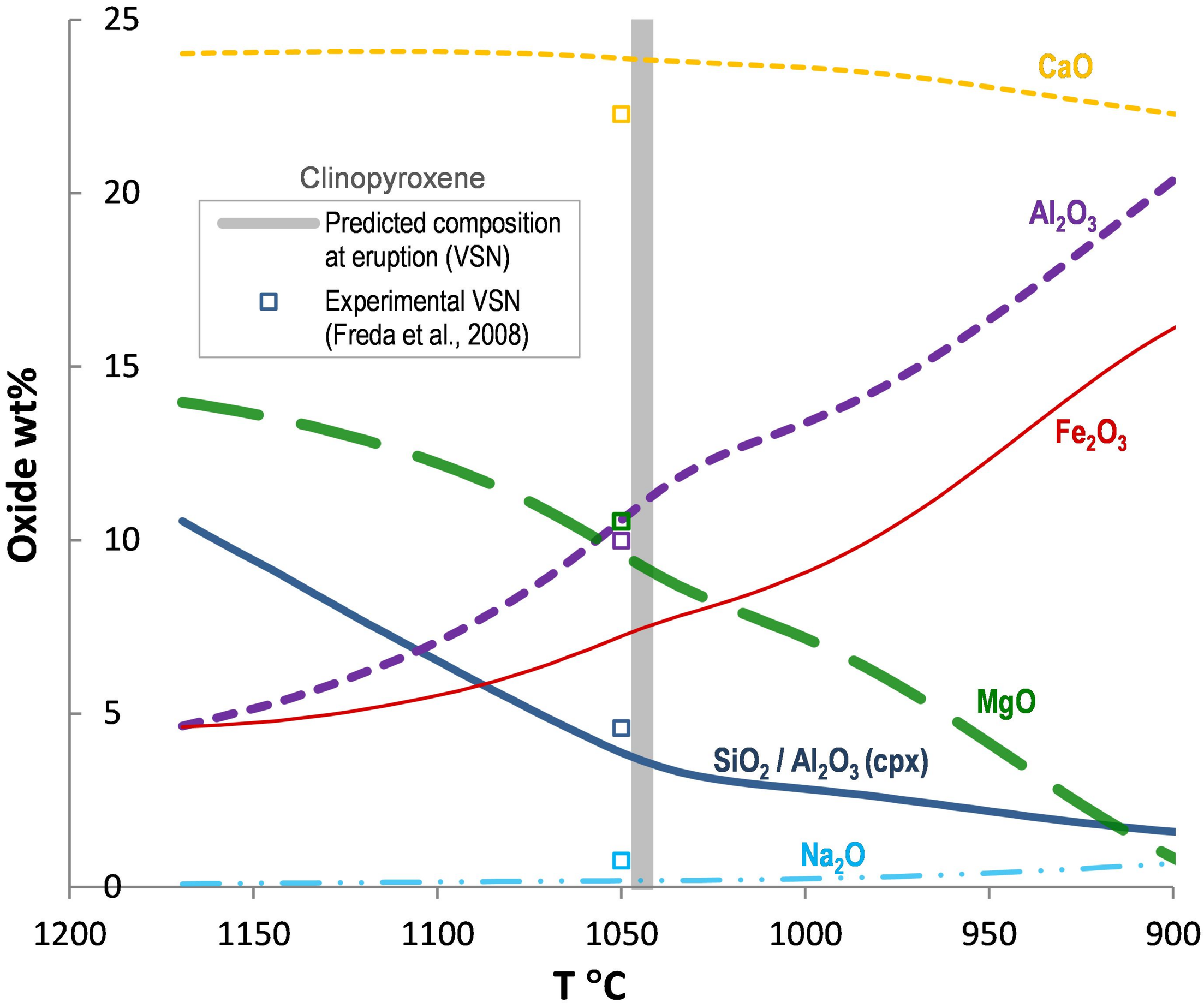
Clinopyroxene
Predicted composition at eruption (VSN)
Experimental VSN (Freda et al., 2008)
CaO
Al2O3
Fe2O3
MgO
SiO2 / Al2O3 (cpx)
Na2O
Oxide wt%
T °C
25
20
15
10
5
0
1200
1150
1100
1050
1000
950
900